Transcriptomic analysis reveals the anti-cancer effect of gestational mesenchymal stem cell secretome

Salvatore Vaiasicca, Gianmarco Melone, David W James, Marcos Quintela, Jing Xiao, Seydou Yao, Richard H Finnell, Robert S Conlan, Lewis W Francis, Bruna Corradetti

Downloaded from https://academic.oup.com/stcltm/article/13/7/693/7641993 by guest on 26 July 2024

Stem Cells Translational Medicine, 2024, **13**, 693–710
https://doi.org/10.1093/stcltm/szae024
Advance access publication 8 April 2024
Original Research

Transcriptomic analysis reveals the anti-cancer effect of gestational mesenchymal stem cell secretome

Salvatore Vaiasicca[1,2], Gianmarco Melone[3], David W. James[3], Marcos Quintela[3], Jing Xiao[4], Seydou Yao[3], Richard H. Finnell[4,5], Robert S. Conlan[3,6], Lewis W. Francis[3], Bruna Corradetti[*,3,4,7]

[1]Advanced Technology Center for Aging Research, IRCCS INRCA, 60124, Ancona, Italy,
[2]Department of Life and Environmental Sciences, Polytechnic University of Marche, 60131, Ancona, Italy,
[3]Centre for NanoHealth, Swansea University Medical School, Singleton Park, SA2 8QA, Swansea, Wales, United Kingdom,
[4]Center for Precision Environmental Health, Baylor College of Medicine, 77030, Houston, TX, United States,
[5]Departments of Molecular and Human Genetics Molecular & Cellular Biology and Medicine, Baylor College of Medicine, 77030, Houston, TX, United States,
[6]Department of Nanomedicine, Houston Methodist Research Institute, 77030, Houston, TX, United States,
[7]Departments of Medicine, Section Oncology, Hematology, Baylor College of Medicine, 77030, Houston, TX, United States

[*]Corresponding author: Bruna Corradetti, PhD MSc, Center for Precision Environmental Health, Baylor College of Medicine, 77030, Houston, TX, United States. (bruna.corradetti@bcm.edu).

Abstract

The environment created during embryogenesis contributes to reducing aberrations that drive structural malformations and tumorigenesis. In this study, we investigate the anti-cancer effect of mesenchymal stem cells (MSCs) derived from 2 different gestational tissues, the amniotic fluid (AF) and the chorionic villi (CV), with emphasis on their secretome. Transcriptomic analysis was performed on patient-derived AF- and CV-MSCs collected during prenatal diagnosis and identified both mRNAs and lncRNAs, involved in tissue homeostasis and inhibiting biological processes associated with the etiology of aggressive cancers while regulating immune pathways shown to be important in chronic disorders. Secretome enrichment analysis also identified soluble moieties involved in target cell regulation, tissue homeostasis, and cancer cell inhibition through the highlighted Wnt, TNF, and TGF-β signaling pathways. Transcriptomic data were experimentally confirmed through in vitro assays, by evaluating the anti-cancer effect of the media conditioned by AF- and CV-MSCs and the exosomes derived from them on ovarian cancer cells, revealing inhibitory effects in 2D (by reducing cell viability and inducing apoptosis) and in 3D conditions (by negatively interfering with spheroid formation). These data provide molecular insights into the potential role of gestational tissues-derived MSCs as source of anti-cancer factors, paving the way for the development of therapeutics to create a pro-regenerative environment for tissue restoration following injury, disease, or against degenerative disorders.

Key words: mesenchymal stem cells; gestational tissues; anti-cancer; transcriptomic analysis; secretome.

Downloaded from https://academic.oup.com/stcltm/article/13/7/693/7641993 by guest on 26 July 2024

Received: 12 September 2023; Accepted: 12 March 2024.
© The Author(s) 2024. Published by Oxford University Press.
This is an Open Access article distributed under the terms of the Creative Commons Attribution-NonCommercial License (https://creativecommons.org/licenses/by-nc/4.0/), which permits non-commercial re-use, distribution, and reproduction in any medium, provided the original work is properly cited. For commercial re-use, please contact reprints@oup.com for reprints and translation rights for reprints. All other permissions can be obtained through our RightsLink service via the Permissions link on the article page on our site—for further information please contact journals.permissions@oup.com.

Graphical Abstract

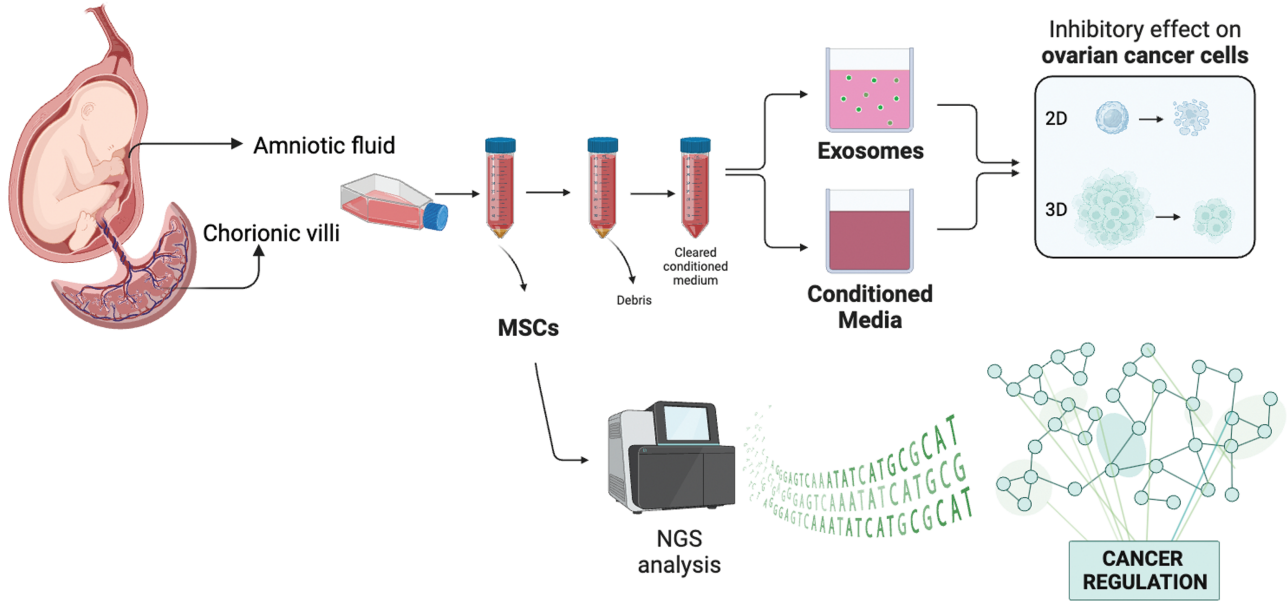

Introduction

The tumor is commonly conceived as the "evil twin of the embryo," due to rapid rates of cellular proliferation and spreading, maternal immune system evasion, and the capability to act as a parasite for nutrient supply.[1] During morphogenesis the precise recapitulation of specific developmental steps and the immature status of the immune system, ensure the correct patterning for tissue growth by the continuous and regulated interplay between neighboring cells.[2] This controlled series of cellular interactions occurs in a well-lubricated environment, where the amniotic fluid (AF) carries proteins and or peptide(s) that can support organogenesis and offer a natural immune response against infections, and the chorionic villi (CV) has an important role in fetomaternal exchanges.[2] The chemical and cellular composition of this environment changes as pregnancy progresses, especially during the 3 gestational inflammatory phases, suggesting their crucial role(s) in protecting and supporting the overall molecular and cellular machinery required for embryo development.[3] While specific mechanisms exploited by mesenchymal stem cells (MSCs) within the uterus to support tissue homeostasis are still under investigation (although homing toward the site of the lesion and the release of paracrine signals have been proposed), several studies have already proven the protective role of AF-derived MSCs isolated from women undergoing healthy pregnancy against the progression of congenital malformations, including spina bifida.[4,5] In AF-MSC-treated groups the exposed spinal area was significantly smaller compared to the controls, concomitantly with a reduction in neural damage.

MSCs derived from fetal adnexa, such as CV and AF, preserve the intermediate properties between adult stem cells and embryonic stem cells, which make them attractive tools for regenerative medicine purposes. More recently, such MSCs have been proposed as tools for the development of potential tumor treatments, as well as the production of factors that may be able to regulate the immune response.[6,7]

Potential MSC roles and functions in cancer are widely debated. Some scientists consider MSCs as carriers of cancer-growth-related factors, sustaining the MSC pro-tumor activity; others have proposed evidence attributing an anti-tumor potential, due to their capability to inhibit the progression of different cancer-related pathways.[8] In both cases, the main players in the communication mechanisms exploited by MSCs to modulate cancer cell responses, are thought to be the paracrine factors they release.[9,10] They include the extracellular vesicles (EVs) and soluble factors (such as growth factors, angiogenic factors, and signaling molecules) which have been shown to play a key role in cell-to-cell communication process.[11,12] EVs, include exosomes (EXO), nanoscopic particles with a lipid/protein shell that confers inherent targeting properties and protect the cargo, constituted by coding and non-coding RNAs with the potential to activate specific phenotypes in recipient cells.[13,14] The chemical and molecular composition of EVs change according to the physiological state and origin of the producer cell, as well as upon exposure to specific environments, meaning that by modulating the microenvironment, whether natural or artificial, it is possible to influence EV features and ultimately their function.[13,15] Based on this premise, together with the fact that the environment created within the placenta during embryogenesis contributes to reducing the frequency of aberrations that drive tumorigenesis, we hypothesize that by understanding the mechanisms exploited by MSCs from tissues harvested at different gestational stages, the AF and CV, it is possible to identify key components useful for the development of naturally inspired anti-cancer therapeutics.

In this study, we demonstrate the anti-tumor potential of MSCs derived from AF- and CV in cell models of High Grade Serous Ovarian cancer. First, we analyzed their transcriptomic profile (genes and lncRNA) looking for factors potentially involved in checkpoint and cancer differentiation processes in target cells, indicating they may be able to play an important role in the cancer maintenance, proliferation, and response to therapy.[16] Second, to validate our hypothesis and mechanism dependence, we performed functional assays to show the anti-cancer effect the CM from AF- and CV-MSCs plays by using ovarian cancer cells, SKOV-3, and OVCAR-3. To better

Downloaded from https://academic.oup.com/stcltm/article/13/7/693/7641993 by guest on 26 July 2024

characterize the role of the paracrine signals produced by AF- and CV-MSCs on tumor cells, we isolated EXOs from the conditioned media, from each cell line, and assessed their potential to inhibit cellular proliferation and induce apoptosis, in SKOV-3 and OVCAR-3 cells.

Materials and methods

Cell lines and cultures

Human chorionic villi (CV) and amniotic fluid (AF) samples for MSC isolation were obtained from healthy pregnant women undergoing chorionic villus sampling and amniocentesis at the Cytogenetic Laboratory Children's Hospital Salesi (Ancona, Italy) upon informed written consent for their use for research purposes. The study was approved by the Regional Institutional Review Board (Comitato Etico Regione Marche) and was conducted in accordance with the Declaration of Helsinki. To obtain MSCs, samples were processed as follows. CVs were carefully separated from maternal decidua using sterile fine forceps to avoid contamination, washed with 1× phosphate-buffered saline (PBS) to remove any blood clots, and subjected to mechanical treatment to obtain small fragments (approximately 3 mm^2 in size). Subsequently, they were transferred into flasks where the cells were allowed to adhere and migrate out of the tissue. AF-MSC samples were obtained from AF (10 mL) and centrifuged at 1200*g* for 10 minutes at room temperature (RT). The supernatant was discarded, and the pellet was washed with PBS to remove any blood clots. This procedure was repeated until the pellet had a clear color. After the cells were cultured in Chang C medium (Irvine Scientific, CA, USA) containing 88% αMEM (Minimum Essential Medium Eagle Alpha Modification; Sigma),10% FBS, 1% GlutaMAX, 100 U/mL penicillin/streptomycin (PS) (Sigma-Aldrich), 10% Chang B Basal Medium, and 2% Chang C supplement (Irvine Scientific) at 37 °C and 5% CO_2. Upon isolation, AF- and CV-MSCs were maintained in Standard Culture Medium constituted by High Glucose-Dulbecco's Modified Eagle Medium (HG-DMEM) (Thermo Fisher Scientific) supplemented with 10% fetal bovine serum (FBS) (Thermo Fisher Scientific), 1% L-glutamine and 100 U/mL PS solution (Sigma–Aldrich).

Ovarian cancer cell lines (SKOV-3 and OVCAR-3) were purchased from ATCC. SKOV-3 cells were cultured in MCCoy's 5A media (Sigma–Aldrich) supplemented with 10% FBS (Thermo Fisher Scientific), 1% L-glutamine, and PS. The OVCAR-3 cell line was cultured in Roswell Park Memorial Institute (RPMI-1640) media (Thermo Fisher Scientific) supplemented with 20% FBS, 1% L-glutamine, and PS. All cell cultures were maintained in incubator at 37 °C with 5% CO_2. The medium was changed twice per week or according to the experiment requirements.

Characterization and proliferation of AF- and CV-MSCs

Morphology

AF- and CV-MSC morphology was evaluated through fluorescence microscopy (Olympus BX51 with SPOT Advanced software). ActinGreen (Life Technologies) and Hoechst (Sigma-Aldrich) were used to specifically highlight the cytoskeleton and nucleus, respectively. Briefly, cells were seeded at 1.4×10^4/well in 300 µL in 8 chamber-slide (Corning BioCoat CultureSlides) and let adhere. Cells were then washed twice in PBS and fixed with 4% paraformaldehyde (PFA) in PBS for 15 minutes. Subsequently, cells were washed another 3 times in PBS. Cells were then permeabilized with 0.1% Triton (in PBS) for 10-15 minutes and washed for a further 3 times wash. MSCs were subsequently blocked in 1% bovine serum albumin (BSA) in PBS for 30 minutes at RT. Cells were then incubated with ActinGreen for 20 minutes and with Hoechst for 5 minutes, at RT. Slides were kept in the dark until observation started.

Cell growth

AF- and CV-MSC growth was evaluated at passage 2 (P2) in 3 biological replicates. MSC were plated at density 10^4 cells/well into 12-well tissue culture polystyrene dishes (EuroClone). Every 2 days, for 15 days, cells were trypsinized and counted by using trypan blue exclusion dye method to evaluate the number and percentage of viability.

Colony forming unit-fibroblast (CFU-F) assay

AF- and CV-MSCs were seeded at P2 passage at different densities (1.5×10^3, 3×10^3, 4.5×10^3 cells/cm^2) in 6-well plates and cultured for 2 weeks as reported. Colonies were subsequently fixed with 1% PFA, stained with Giemsa at RT, and washed. Colonies formed by 15-20 nucleated were counted with inverted microscope (Meiji Techno).

Expression of MSC-associated markers

AF- and CV-MSCs were analyzed at P2. For flow cytometry analysis, cells were trypsinized, washed in PBS, and fixed with 75% ethanol overnight at −20 °C. Cells were subsequently centrifuged at 700*g* for 7 minutes, washed in PBS, and incubated for 20 minutes in 0.5% BSA in PBS to block all the non-specific sites. Aliquots containing 5×10^5 cells each were resuspended in PBS and centrifuged at 500*g* for 5 minutes at 20 °C. The supernatant was then discarded, and cells were stained with fluorescently labeled antibodies following manufacturers' instructions. The following directly conjugated antibodies were used: phycoerythrin (PE)-conjugated ecto-*5′*-nucleotidase (PE-*CD73*; Biolegend), fluorescein isothiocyanate (FITC)-conjugated thymocyte differentiation antigen 1 (FITC-*CD90*; Biolegend) and the glycoprotein *CD44* (FITC-CD44; Biolegend), allophycocyanin (APC)-conjugated for integrin b1 (APC-*CD29*; Biolegend). Incubation was performed for 45 minutes at RT in the dark. Cells were washed twice with filtered PBS to remove antibodies in excess and for each sample was detected 10 000 events using Guava Easycyte Millipore flow cytometer with GuavaSoft 2.2.3 software. For both cell lines, the control group (represented by unstained cells) was compared to its treated (represented by stained cells). Gene expression analysis was performed on AF-MSCs to determine the expression of pluripotent (*Nanog* and *Oct-4*)-, mesenchymal (*Cd105*, *Cd90*, *Cd44*, and *Cd73*), hematopoietic (*Cd45* and *Cd34*)-associated markers. Total RNA was extracted from cells using TRI Reagent (Sigma–Aldrich, St. Louis, Missouri, United States) according to the manufacturer's instructions. RNA concentration and purity were measured by Nanodrop Spectrophotometer (Nanodrop ND1000). cDNA was synthesized from 500 ng total RNA using a PrimeScript RT-Reagent Kit (Takara). Gene expression was evaluated using human-specific oligonucleotide primers (Table 1,[17]). Primers used were designed using open-source Primer-BLAST, across an exon–exon junction to avoid genomic

Downloaded from https://academic.oup.com/stcltm/article/13/7/693/7641993 by guest on 26 July 2024

Table 1. Nucleotide sequence, melting temperature, and transcript length of primers used to evaluate the expression of mesenchymal, hematopoietic, and pluripotent genes.

Gene	Sequences (5′→3′)	T_m (°C)	Product size (bp)
Mesenchymal markers			
CD44 molecule (*Cd44*)	S: GGAGCAGCACTTCAGGAGGTTAC A: GGAATGTGTCTTGGTCTCTGGTAGC	63	129
5′-Nucleotidase, ecto (*Cd73*)	S: GCTCTTCACCAAGGTTCAGC A: GTGGCTCGATCAGTCCTTCC	59	203
Thy-1 cell surface antigen (*Cd90*)	S: CTTTGGCACTGTGGGGGTGC A: GATGCCCTCACACTTGACCAG	61	211
Endoglin (*Cd105*)	S: CCTGGAGTTCCCAACGGGCC A: GGCTCTTGGAAGGTGACCAGG	62	186
Hematopoietic markers			
CD34 molecule (*Cd34*)	S: GTGTCTACTGCTGGTCTTGG A: CAGTGATGCCCAAGACAGC	58	200
CD45 molecule (*Cd45*)	S: GACAACAGTGGAGAAAGGACG A: GCTGTAGTCAATCCAGTGGGG	60	170
Pluripotent markers			
Pou class 5 homeobox 1 (*Oct-4*)	S: CGATCAAGCAGCGACTATGC A: AGAGTGGTGACGGAGACAGG	60	200
Nanog homeobox (*Nanog*)	S: GCAAGAACTCTCCAACATCC A: GGTCTGGTTGCTCCACAT	56	178
Differentiation (osteogenesis and adipogenesis) markers			
RUNX family transcription factor 2 (*Runx2*)	S: GGTTAATCTCCGCAGGTCACT A: CACTGTGCTGAAGAGGCTGTT	60	143
Bone gamma-carboxyglutamate protein (*Bglap*)	S: TCACACTCCTCGCCCTATTG A: TCGCTGCCCTCCTGCTTG	68	78
Adiponectin (*Adipoq*)	S: CCCAAAGAGGAGAGAGGAAGCT A: GCCAGAGCAATGAGATGCAA	60	73
Leptin (*Lepr*)	S: CCAAAACCCTCATCAAGACAATT A: AGTCCAAACCGGTGACTTTCTG	58	90
Reference gene			
Glyceraldehyde-3-phosphatase dehydrogenase (*Gapdh*)	S: TCCACTGGCGTCTTCACC A: GGCAGAGATGATGACCCTTT	68	78

S = sense primer, A = antisense primer, T_m = melting temperature, bp = base pairs.

DNA amplification and make manual corrections to make better amplification. Quantitative PCRs were performed with SYBR green method in a StepOneTM Real-Time PCR System, StepOne cycler software v2.3. Triplicate PCR reactions were carried out for each sample analyzed. Human glyceraldehyde-3-phosphate dehydrogenase (*Gapdh*) was employed as a reference gene in each sample to standardize the results by eliminating variation in cDNA quantity.

MSC differentiative potential

To test their multipotent differentiative potential, AF- and CV-MSCs at P3 were seeded at a density of $1 \times 10^3/cm^2$ in 6-well tissue culture dishes. For osteogenesis, cells were cultured in HG-DMEM, supplemented with 10% FBS, 100 U/mL penicillin, 100 µg/mL streptomycin, 0.25 µg/mL amphotericin B, 2 mM/L L-glutamine, 10 mM β-glycerophosphate (Sigma, 50020), 0.1 µM dexamethasone (Sigma, D2915), and 250 µM ascorbic acid (Sigma, A8960). For adipogenic differentiation, cells were cultured in HG-DMEM, supplemented with 10% FBS, 100 U/mL penicillin, 100 µg/mL streptomycin, 0.25 µg/mL amphotericin B, 2 mM/L L-glutamine, 10 µg/mL insulin (Sigma I-6634), 150 µM indomethacin (Sigma I-7378), 1 µM dexamethasone, and 500 µM IBMX (3-isobutyl-methyl-xanthine, Sigma I-7018). Induced cells were incubated for 2 weeks at 38.5 °C with 5% CO_2. Non-induced control cells were cultured for the same time with standard medium (HG-DMEM supplemented with 10% FBS, 100 U/mL penicillin, 100 µg/mL streptomycin, 0.25 µg/mL amphotericin B, 2 mM/L L-glutamine). The presence of calcium deposits in differentiated cells was verified after 14 days of induction by Alizarin Red staining, whereas Oil Red O staining was used to identify lipid droplets in the cytoplasm. Expression of specific genes was performed as reported in Expression of MSC-associated markers section to confirm the occurred differentiation.

RNA sequences analysis by Next Generation Sequencing

RNA extraction and quality check

Total RNA was extracted from AF- and CV-MSCs at P2 using the total RNA Purification Plus Kit (Norgen) and processed by the Functional Genomic Center (University of Verona, Italy). RNA concentration and integrity were assessed using the RNA 6000 Nano Kit (Agilent Technologies). RNA samples showed an integrity number (RIN) > 9 [17].

Downloaded from https://academic.oup.com/stcltm/article/13/7/693/7641993 by guest on 26 July 2024

RNA-seq library preparation

RNA-seq library preparation was performed using the TruSeq stranded mRNA kit (Illumina) from 1 µg of RNA per sample. Library size was assessed by capillary electrophoretic analysis with the Agilent 4200 Tape station. RNA libraries were analyzed on an Illumina NextSeq 500 sequencer using 75nt single reads. The quality of the reads was checked using software FastQC (http://www.bioinformatics.babraham.ac.uk/projects/fastqc/), discarding those reporting more than 50 bp with low scores. Subsequently, through the software Scythe (https://github.com/vsbuffalo/scythe) adaptor contamination was removed, and the reads showing low-quality ends were trimmed or removed using the software Sickle (https://github.com/vsbuffalo/sickle). Filtered reads were aligned to the Human reference genome GRCh38 using HISAT2 [15]. Gene count normalization and differential analysis were performed using the R bioconductor package DESeq2,[18] contrasting AF-MSC samples (x3) with CV-MSC (x3) for all transcripts samples. Raw and processed data are deposited in the Gene Expression Omnibus (GEO) database with accession number GSE240855. Protein-coding genes and long non-coding RNAs were selected from the differential analysis results for further analysis. Genes that exhibited high expression in both AF-MSCs and CV-MSCs. Transcripts with high expression in both MSC populations were identified by finding genes without significant differential expression (*P* adjusted > .05) and having total normalized gene counts of > 100.

Secretome analysis

A list of 1904 predicted secreted proteins was obtained from the human protein atlas (HPA) by querying the protein class for "Predicted secreted proteins."[19] Differential analysis results for "secretome" transcripts were selected from the total differential analysis.

Principle component analysis

Principle component analysis was performed on the normalized gene counts using R prcomp function. Results were plotted using ggplot2 R package.

Heatmap and volcano plot

Differentially expressed genes (DEGs), heatmap, and volcano plots between AF- and CV-MSCs were created using ggplot2 package. The criteria of DEGs were adjusted *P*-value (*P*adj) < .05 and $|\log_2$ fold change| > 1.

Pathway and gene ontology

Significantly enriched pathways for DEGs between AF-MSCs and CV-MSCs secretome genes and genes with common high expressions were identified using the WebGestaltR package to perform gene set enrichment analysis (ORA). All HPA secretome genes were used as background for protein-coding and secretome analyses respectively. ORA analysis was applied to KEGG,[20] GO biological processes[21], and mSigDb onco hallmarks.[22] Lnc-related enriched KEGG pathways for upregulated, downregulated, and common highly expressed lncs were identified using lncPath package.[23]

Effect of the media conditioned by AF- and CV-MSCs on ovarian cancer cell viability

Conditioned media preparation

Conditioned media was collected from AF- and CV-MSCs at passages from 1 to 4. Briefly, MSCs were cultured at the density of 1×10^4 cell/cm^2 in standard culture medium until 70% of confluence. The media then was replaced with standard medium containing exosomes depleted FBS and cultured for additional 48 hours. At the end of the culture period, CM was collected, centrifuged at 500*g*, filtered through a 0.45 µm pore size, and kept at −80 °C until use.

Cell viability in 2D conditions

The effect of CM obtained by AF- and CV-MSCs was evaluated on SKOV-3 and OVCAR-3, through RealTime-Glo MT Cell Viability Assay (Promega). Briefly, SKOV-3 and OVCAR-3 cells were plated in 96-well plates at the density of 1×10^3 and 5×10^3 cells/well, respectively. Cells were subsequently exposed to AF-CM and CV-CM for 72 hours and analyzed following manufacturer's indications. Experiments were performed in 3 independent biological replicates and the results expressed in percentage (%) were compared to control groups represented by untreated cells.

Cell viability in 3D conditions

The cytotoxic effect of the CM obtained from AF- and CV-MSCs on cancer cells was also evaluated using 3D culture system, through the CellTiter-Glo 3D Cell Viability Assay (Promega, Madison). Spheroids were generated from both ovarian cancer cell lines plated at 5×10^3 cells/well in spheroid microplate 96-well plates (Corning Incorporated) over a 24-hour period. Cells were then treated with AF- and CV-CM for 72 hours and analyzed following manufacturer's indications. Experiments were performed in 3 independent biological replicates and the results expressed in percentage were compared to control groups represented by untreated cells.

Effect of AF- and CV-MSC CM on ovarian cancer spheroid formation

AF- and CV-CM effects on cancer cells (OVCAR-3 and SKOV-3) spheroids formation and maintenance were evaluated following 3 methods of exposure: *Method 1*. Cancer cells exposure to CM before spheroid formation. *Method 2*. Cancer cells exposed to CM after spheroid formation (conventional method). *Method 3*. Cancer cells exposed to CM during spheroid formation. Briefly, *Method 1:* OVCAR-3 and SKOV-3 were plated 1×10^3 and 5×10^3 cells/cm^2, respectively, in 24-well plates and let adhere. After 24 hours, spheroids were treated with CM for 72 hours. At the end of the treatment period cells were trypsinized and plated in spheroid microplate 96-well plates (Corning Incorporated) for 24 hours. *Method 2:* Cells were plated at 5×10^3 cells/well in spheroid microplate 96-well plates. After 24 hours spheroids were treated with AF- and CV-CM for 72 hours. *Method 3:* Cancer cells were plated at 5×10^3 cells/well spheroid microplate 96-well plates and incubated with CM for 72 hours. Spheroids obtained from each experimental condition were imaged. At least 3 different independent spheroids were captured by using light microscopy (Zeiss Primo Vert). The images were captured at 4× magnification, and their morphological parameters were analyzed using free-source AnaSP software after making binary masks of spheroids images through MATLAB software.

Isolation and characterization of exosomes from AF- and CV-MSCs

Exosomes isolation

Exosomes were isolated from AF-CM (AF-EXO) and CV-CM (CV-EXO) using the ExoQuick-TC (System Biosciences)

Downloaded from https://academic.oup.com/stcltm/article/13/7/693/7641993 by guest on 26 July 2024

according to manufacturer instructions. Briefly, CM was collected and subjected to serial centrifugations at 3000*g* for 15 minutes to remove cells and debris. The supernatant was recovered and used for the extraction. ExoQuick-TC reagent was added to the media and mixed by inverting the tubes several times. The mixture was incubated overnight at 4 °C and centrifuged at 3000*g* at 4 °C. Isolated exosomes were resuspended in 0.2 µm-filtered PBS buffer and kept at −80 °C until further experiments.

Nanoparticle tracking analysis (NTA)

Exosome (EXO) concentration and size were analyzed in scatter mode by Nanoparticle Tracking Analysis (ParticleMetrix) with ZetaView software. Briefly, EXO suspension obtained from AF- and CV-MSCs was diluted 1/10 in PBS. To detect EXO in the recommended margin (50-200 nm particles) the setting instrument had 50 and 70 for sensitivity and shutter, respectively. In addition, the specifical features used to collect data (size distribution and concentration) were 30 frames/seconds for 11 positions.

Scanning electron microscopy

In the process of analyzing EXO using a scanning electron microscope (SEM), 5 µL of the sample at a concentration of 1×10^9 particles per milliliter was deposited onto silicon wafer chips (Ted Pella Inc., United States). These chips were pre-functionalized for 2 hours with 1% (3-aminopropyl) triethoxysilane (Sigma–Aldrich, United States) in ethanol, with the addition of 1% distilled water for catalysis. Subsequently, the chips loaded with samples underwent 3 cycles of 10 µL ethanol deposition and a final deposition of 50% butanol. Each deposition was carefully absorbed using wipes (Kimtech Science, United States), and all fluids were thoroughly dried by blowing air. A 2 × 2 cm Petri dish piece was mounted with double-side carbon tape (Ted Pella Inc., United States) on an aluminum SEM stub (Ted Pella Inc., United States). A Nava Nano SEM 230 (Thermal Fisher, United States) was used to image samples. All SEM experiments were performed at RT (22 °C) and under a high vacuum range (5×10^6 to 2×10^6 Torr). The accelerator voltage was set at 5-7 kV for imaging. The electron beam spot-size was set at 3 nm and the working distance was 5 mm.

Effect of AF- and CV-EXO on ovarian cancer cells

Exosome internalization by cancer cells

To track them upon internalization AF- and CV-EXO were stained with Vibrant DiD cell labeling solution (Thermo Fisher Scientific) following manufacturer's instructions. Briefly, 100 µL of exosome suspension was stained with 0.5 µL of Vibrant DiD (1:200 dilution) and incubated for 20 minutes at 37 °C in the dark. Fluorescently labeled-EXO was administered to SKOV-3 and OVCAR-3 cells 10^5 exosomes. Internalization was confirmed by confocal microscopy LSM-710 microscope (Carl Zeiss) after 24 hours of exposure.

Cytotoxic effect of exosomes on ovarian cancer cells

The effect of AF- and CV-EXO on SKOV-3 and OVCAR-3 cells was evaluated by RealTime-Glo Annexin V Apoptosis and Necrosis Assay (Promega). Briefly, cancer cells were seeded in 96 well/plate at the concentration of 1×10^3/well and 5×10^3/well, respectively, and let adhere. Subsequently, they were treated with 10^6 AF- or CV-EXOs for 72 hours. Annexin V and necrosis detection components were then prepared following the manufacturer's indications to evaluate any apoptotic effect induced by the exosomes. Emitted luminescence signal of the annexin V binding and molecular factor related to necrosis was detected with a plate-based multimode reader. As positive control, Staurosporine (Sigma–Aldrich) at 2 nM concentration was used. The apoptotic processes were monitored and recorded every 24 hours by Spectrophotometer (SPECTROstar Omega) using MARS data analysis software. Early (luminescent signal) and late (fluorescent signal) apoptotic cells were expressed in percentage compared to untreated cancer cells (CTRL).

Statistical analysis

Statistical analysis was performed using GraphPad Instat 3.00 for Windows (GraphPad Software). Three biological replicates for each experiment (viability, differentiative potential, apoptosis, spheroid analyses, and NTA) were performed and the results are reported as average ± SD. One-way analysis of variance for multiple comparisons by the Student–Newman–Keuls multiple comparison test was used to assess differences between groups. Differences were considered statistically significant for P values < .05.

Results

Isolated AF- and CV-MSCs display typical MSC features

Upon isolation, comprehensive characterization of AF- and CV-MSCs was performed in terms of morphology, proliferation, and expression of specific mesenchymal markers. MSCs from different sources display distinctive shapes, with cobblestone-like morphology for AF-MSC and fibroblast-like one for CV-MSCs (Figure 1A). Growth curves show AF- and CV-MSCs display similar lag phase (3 days). During the exponential growth phase (log phase 3-13 days) both cell lines exhibited variable proliferative trends (Figure 1B). CV-MSCs showed statistically significantly increased proliferation compared to AF-MSCs from days 3 to 9 ($P < .05$). At day 12 AF-MSC growth becomes more robust, reaching an almost 3-fold increase compared to their CV counterparts ($P < 0.01$). Both cell lines demonstrate clonogenicity (Table 2), as shown by directly correlation between the increase in CFU frequency and the increase in cell seeding density. Flow cytometry, in both cell lines, revealed a high positivity for MSC-associated markers, including CD29, CD73, CD90, and CD44 (97% ± 2 on average, Figure 1C). Molecular analysis confirmed typical mesenchymal phenotype, with expression of pluripotent (*Nanog, Oct-4*)- and adult MSC (*Cd73*, *Cd90, Cd44, Cd105*)-markers. No blood cell contamination was detected, as demonstrated by the lack of expression of the hematopoietic markers (*Cd34* and *Cd45*) (Figure 1D).

AF and CV-MSCs show differentiative potential

Before proceeding with transcriptomic analyses, AF and CV-MSC samples were also tested for differentiative potential (Figure 1E). Over 2 weeks of culture in osteogenic induction medium, both cell lines distinctly changed their morphology and were surrounded by calcium deposits positive to von Kossa staining. Expression of osteogenesis-associated genes confirmed the occurred differentiation in both cell types (Figure 1E, a) with CV-MSCs showing a more marked specification process. Expression of the transcription factor

Downloaded from https://academic.oup.com/stcltm/article/13/7/693/7641993 by guest on 26 July 2024

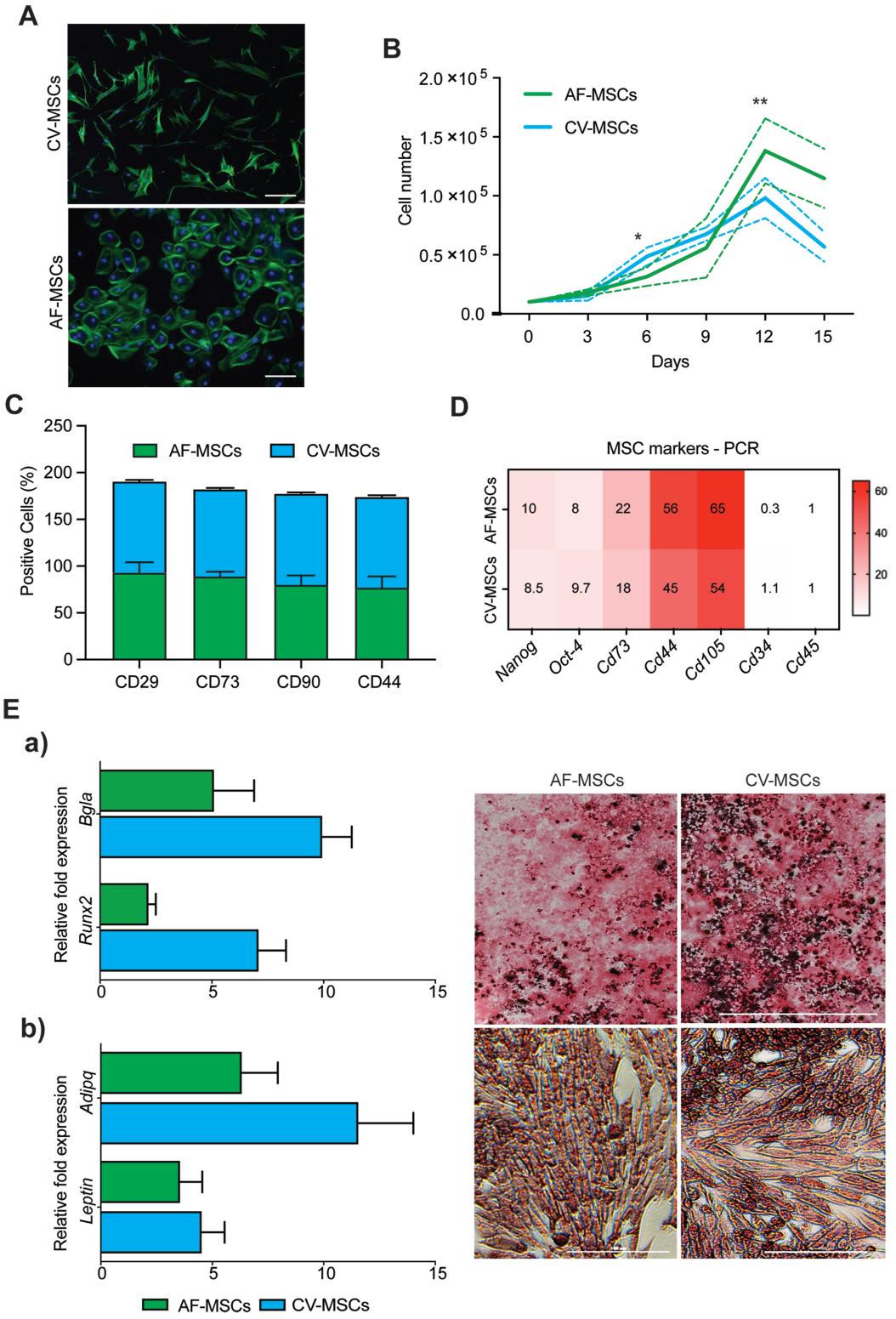

Figure 1. AF- and CV-MSC characterization. (A) Representative fluorescent microscopy images showing CV- and AF-MSC morphology. F-actin structures highlighted by ActinGreen staining and nuclei by Hoechst. 20× magnification, scale bar = 10 μm. (B) Growth curves obtained from AF- and CV-MSCs over a 15-day period. Results are reported as average of 3 biological replicates ± SD. (C) Percentage of cells positive for the MSC-associated markers studied (CD29, CD73, CD90, and CD44) in AF- and CV-MSCs as revealed by flow cytometric analysis. Results are presented as average of 3 biological replicates ± SD. (D) Heatmap showing the results obtained from quantitative PCR analysis performed to evaluate pluripotent (*Nanog, Oct4),* mesenchymal (*Cd73*, *Cd90*, *Cd44*, and *Cd105*), and hematopoietic markers in AF- and CV-MSCs at passage P2. Expression levels normalized to the internal control, *Gapdh* ($n = 3$). (E). AF- and CV-MSC osteogenic (a) and adipogenic (b) differentiation after 14 days of induction. Osteogenesis was confirmed by Alizarin Red staining to highlight mineral deposition and adipogenesis by Oil-red-O positive cytoplasmic neutral lipids. Expression levels of osteogenic markers, (*Runx-2* and *Bglap*) and (*Lepr* and *Adipq*) were determined by quantitative qRT-PCR. Data were normalized to the reference gene (*Gapdh*) and represented as fold-change compared with the expression untreated AF- or CV-MSCs. Values are mean ± SD ($n = 3$). Asterisks depict significance (*$P < 0.01$).

Downloaded from https://academic.oup.com/stcltm/article/13/7/693/7641993 by guest on 26 July 2024

Runx-2 was assessed around 2.16 ± 0.33 and 7.08 ± 1.23 for AF- and CV-MSCs, while the expression of the osteogenic marker *Bglap* showed values assessed around 5.09 ± 1.8 and 9.93 ± 1.32, respectively. In controls, the same changes were not observed. Both cell lines were found to differentiate into adipocytes (Figure 1E), as shown by the presence of lipid vacuoles. Gene expression confirmed occurred differentiation and significant extents between the 2 cell lines. Expression of the transcription factor *Adipq* was found to be significantly increased compared to control, with values assessed at 6.32 ± 1.62 and 11.54 ± 2.47 for AF and CV-MSCs, respectively, while the expression of the adipogenesis-associated marker *Leptin* was found to be 3.55 ± 1.00 and 4.52 ± 1.034 for the same samples.

Transcriptomic analysis

RNA extraction and quality check

RNA samples extracted from AF and CV-MSCs showed an integrity number (RIN) > 9, with no significant difference in raw and aligned reads obtained across the 3 biological replicates, confirmed by ANOVA (>0.99). As reported in Table 3, ~31 million reads were considered for each sample with filtered reads mapped to ~99% of the Human reference genome used (GRCh38).[17]

Protein-coding differential gene expression analysis

PCA analysis of normalized gene expression, for protein-coding genes, shows a clear separation of AF-MSC and CV-MSC samples (Figure 2A). Differential analysis of RNA-seq data comparing AF-MSCs with CV-MSCs reveals 2505 significantly upregulated and 1901 significantly downregulated protein-coding genes (P adjusted < .05) (Figure 2B). In addition, we found 5226 genes that have high expression in both AF- and CV-MSC samples. The top 30 up and downregulated protein-coding genes, from AF- and CV-MSCs, are shown in Figure 2C. Performing pathway analysis for significantly dysregulated genes did not reveal any significantly enriched pathways.

Differential analysis of secreted protein-coding genes

To understand the effect which these cell types may have on surrounding cells and tissue, we isolated proteins in the differential expression results which are known to be secreted by cells, (ie, the secretome) from our protein-coding gene selection. PCA analysis of normalized gene expression for secretome genes still showed a clear separation between AF- and CV-MSCs (Figure 3A). We found that 245 and 174 genes encoding secreted proteins are significantly up and downregulated respectively, as shown in Figure 3B. A further 269 have high expression levels in both cell types. The top 30 up and downregulated genes are shown in Figure 3C. For genes that exhibit high expression in both MSC types, we found pathways enriched related to angiogenesis, regulation of inflammatory response, regulation of endothelial cell proliferation pathways, and TGF pathways (Figure 4A). Interestingly, significant enrichment of Wnt signaling was observed. Specifically, pathway analysis of dysregulated and commonly expressed genes revealed enrichment of cell growth and TGF pathways, in the upregulated AF secreted proteins. Negative regulation of pathways linked to cellular component movement, negative regulation of transmembrane receptor protein serine/threonine kinase signaling pathway, and positive regulation of angiogenesis pathways, were enriched in the upregulated CV-secreted proteins (Figure 4A).

Long non-coding (lnc) RNAs

The dysregulated lncRNAs found were mapped between AF-MSCs and CV-MSCs, showing high expression in both cell types. Subsequent KEGG pathway analysis was performed, to understand how lncRNAs secreted by these cells may regulate the function of neighboring cells and tissues (Figure 4B). Cell cycle, apoptosis, and TGF pathways were again enriched for, in lncRNAs highly expressed in both cell types. Interestingly, we found an enrichment of several cancer-related pathways in lncRNAs upregulated in the AF-MSC samples, as well as gap junction proteins. While chemokine signaling and B-cell receptor pathways were enriched in upregulated CV-MSC lncRNAs (Supplementary Table S1).

PCA analysis of lncRNAs in both cell types shows a clear separation between AF- and CV-MSCs (Figure 5A). Further, 1156 non-coding RNAs show a high expression in both cell types with 914 and 842 antisense and lncRNA respectively (Supplementary Table S2). We find that 258 and 180 lncRNAs are significantly up and downregulated respectively, as shown in Figure 5B. The top 30 up and downregulated lncRNAs are shown in Figure 5C.

AF- and CV-CM impair ovarian cancer cell viability in 2D and 3D culture systems

Treatment with CM derived from AF- and CV-MSCs had an impact on SKOV-3 and OVCAR-3 cell lines, reducing their

Table 2. Clonogenicity potential of AF- and CV-MSCs as revealed by the colony forming unit-fibroblast like (CFU-F) assay.

Cell type	Cell density/cm² (×10³)	Total cells (×10³)	CFU-F	1 CFU each (×10³)
AF-MSCs	1.5	12.3	2.5 ± 0.7	7.1
	3.0	28.5	4.0 ± 0.4	5.7
	4.5	42.7	10.5 ± 0.7	4.2
CV-MSCs	1.5	14.7	4.0 ± 1.4	15.8
	3.0	55.0	7.5 ± 0.4	11.8
	4.5	85.0	12.5 ± 0.7	12.6

Table 3. Gene reads obtained during the NGS analysis of amniotic fluid (AF-MSCs) and chorionic villi (CV-MSCs) isolated from women.

Cell type	Total reads	Mapped reads (%)	Unique mapping (%)	Multimapping reads (%)
AF-MSCs	31,636,889	98.99	90.72	8.27
	32,260,591	99.01	90.68	8.32
	32,892,229	99.01	90.76	8.25
CV-MSCs	32,119,080	99.04	91.24	7.81
	29,440,066	99.02	90.16	8.86
	330875473	99.03	90.76	8.27

Raw and aligned reads indicate the reads before and after the bioinformatics processes, respectively. 3 biological replicates were considered in the analysis.

Downloaded from https://academic.oup.com/stcltm/article/13/7/693/7641993 by guest on 26 July 2024

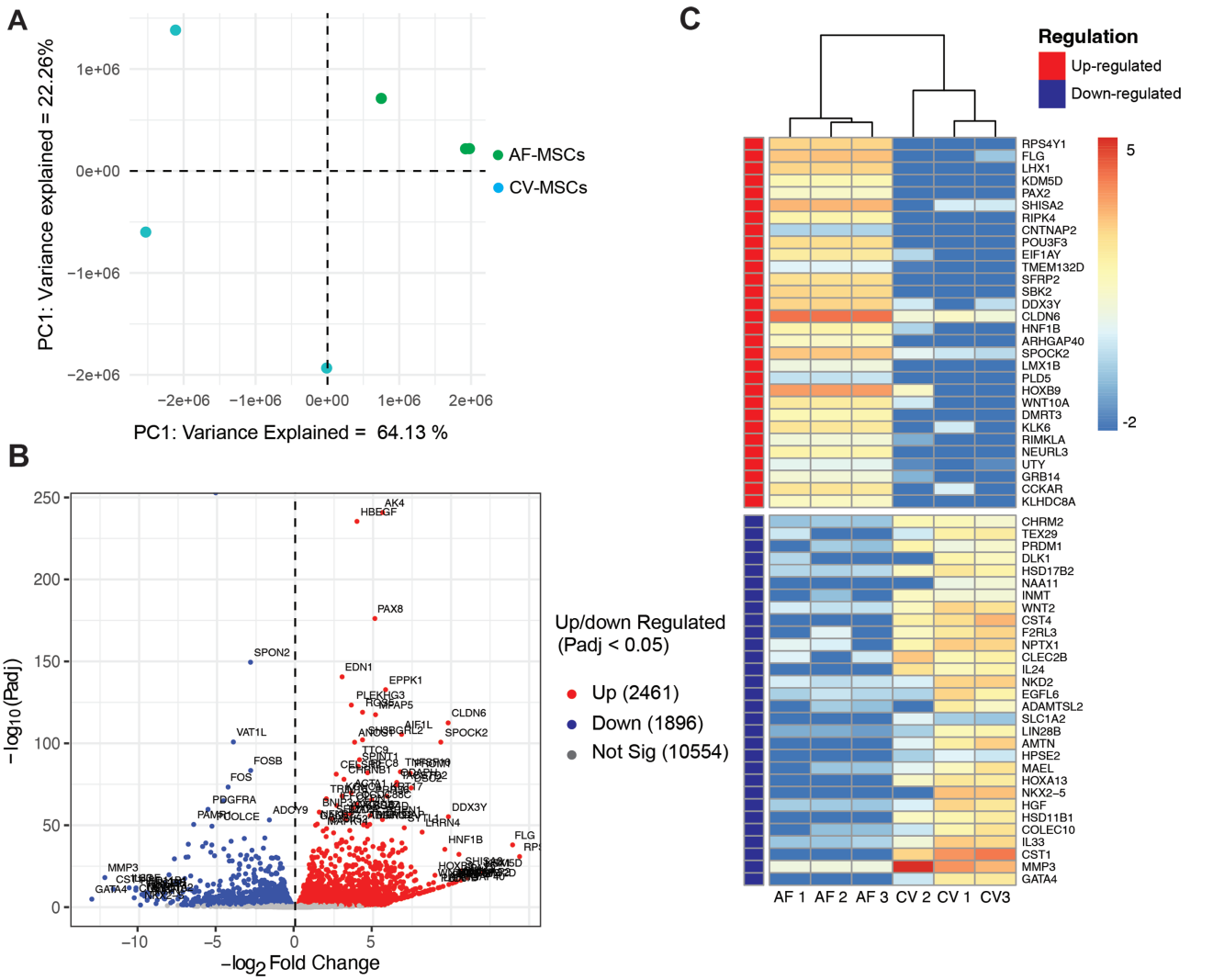

Figure 2. Transcriptome analysis reveals DEG between AF- and CV-MSCs. (A) PCA plot shows the separation between AF-MSC and CV-MSC samples and the similarity among the replicates. (B) Volcano plot displaying the log fold change and *P*-value of genes in AF samples against CV samples. Significantly upregulated downregulated genes are reported (*P*adj < .05). Genes where *P*adj > .05 are also shown. (C) Hierarchical clustering heatmap showing top 30 up and top 30 downregulated genes from all differentially expressed genes (*P* adjusted < .05) for AF- and CV-MSCs. Dendrograms show hierarchical clustering results.

viability. As shown in Figure 6A, a significant decline was observed in both cell lines following 72-hour exposure to AF- and CV-CM, with 98% ± 1.5 and 85.5% ±3 reductions for SKOV-3 cells, respectively ($P < .05$). A similar trend was observed in OVCAR-3 with a reduction of 88% ± 1.7 and 88% ± 6.4 ($P < 0.01$) and for AF- and CV-CM, compared to untreated cells (CTRL). Stem cell standard culture medium (media only group) also affected cancer cell viability, with a reduction of 57% ± 2 for SKOV-3 and 63% ± 1.8 for OVCAR-3. When the effect of AF- and CV-CM was evaluated in 3D, a similar trend was displayed (Figure 6B). In SKOV-3 a significant ($P < .01$) reduction was revealed after exposure to AF-CM, assessed around 56% ± 8.2 compared to CTRL which was not evident in CV-CM. On the other hand, the reduction of cell viability in OVCAR-3 cells was 42.4% ± 9. 27% ± 3.7, and 16% ± 13 for AF-CM and CV-CM compared to CTRL. Spheroids exposed to only media did not show a significant reduction in viability compared to the controls.

AF- and CV-CM affects spheroid formation, length, and sphericity

The analysis of the effect of AF- and CV-CM on SKOV-3 and OVCAR-3 spheroids revealed significant changes in the area, length, and sphericity. In SKOV-3 significant ($P < .05$) and highly significant ($P < .01$) decrease of spheroid area following the treatment with AF-CM was noted, with 3400.83 ± 63.41 μm² and 6360 ± 1532.9 μm² for *Method 1* and *Method 2*, respectively, compared to untreated cells (CTRL) (Figure 6C). No significant differences were observed in spheroid area following the treatment with CV-CM except for a slight increase with *Method 1*. In OVCAR-3 cells, a significant ($P < 0.01$) reduction in spheroid area and length has been observed following *Method 1* and *Method 2* with both, CV- and AF-CM treatment. In particular, the spheroid area decreases to approximately 1.7e⁴ ± 1919.3 and 1.8e⁴ ± 971.9 μm² for CV- and AF-CM, respectively, with *Method 1*, and 1.1e⁴ ± 4392.4 and 1.2e⁴ ± 1646.1 μm² for CV- and AF-CM, with *Method 2*. A similar trend is observed in terms of

Downloaded from https://academic.oup.com/stcltm/article/13/7/693/7641993 by guest on 26 July 2024

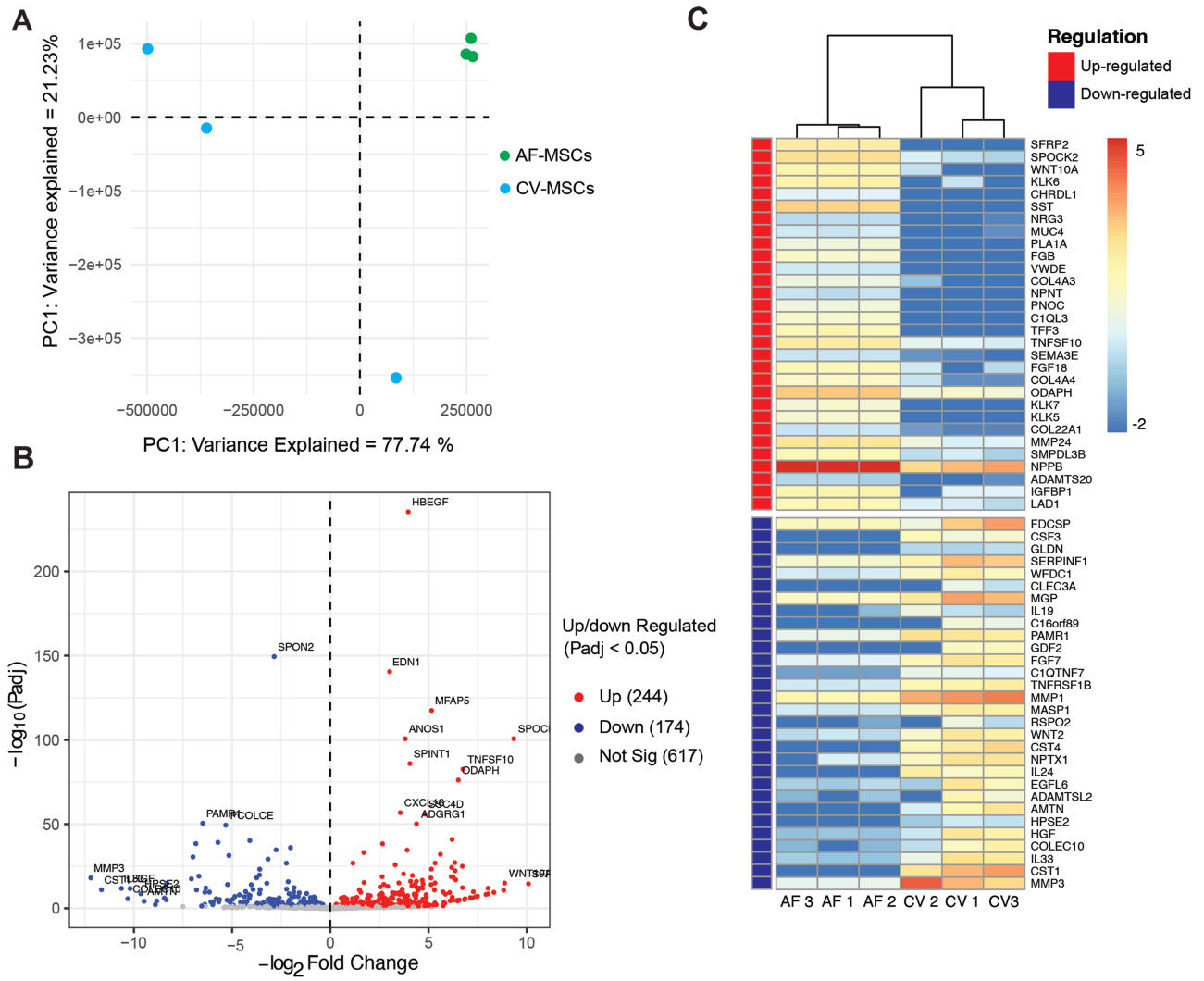

Figure 3. Differentially expressed secreted protein-coding genes. (A) PCA plot analysis of normalized gene expression for secretome genes shows a clear separation between AF- and CV-MSCs. (B) Volcano plot displaying the log fold change and *P*-value of expressed secreted protein in AF samples against CV samples. Significantly upregulated and downregulated genes are reported (*P*adj < 0.05). Genes where *P*adj > 0.05 are also shown. (C) Hierarchical clustering heatmap showing top 30 up and top 30 downregulated differentially expressed secreted protein-coding genes (*P* adjusted < .05) for AF- and CV-MSCs. Dendrograms show hierarchical clustering results.

spheroid length (Supplementary Figure S1A). A significant reduction ($P < .01$ and $P < .01$) was observed after treatment with CV- and AF-CM following *Method 1* (47.64 ± 10.7 and 52.39 ± 3.2, respectively) while *Method 2* recorded a decrease of 36.9 ± 9.2 and 35.6 ± 8.02 for CV- and AF-CM, respectively (Supplementary Figure S1B). Both cell lines did not form spheroids following the exposure to AF- and CV-CM through *Method 3*, as demonstrated by the fragmented appearance of the spheroids shown in Figure 6D.

Exosomes derived from AF- and CV-MSCs differentially affect ovarian cancer cell viability and apoptosis

Exosomes derived from AF- (AF-EXO) and CV-MSC (CV-EXO) were characterized by NTA to determine concentration and size (Figure 7). No differences between AF- and CV-EXO were found in terms of size (Figure 7A), with values (expressed in nm) assessed around 117.42 ± 21 and 125 ± 32 for AF- and CV-EXO, respectively. Through SEM analysis, 3-dimensional morphological images of EXOs from both cell types were generated showing a spheroidal shape (Figure 7B). A significant difference ($P < .01$) was observed in the number of exosomes released by the 2 cell lines, with $2.17 \times 10^{10} \pm 1.10 \times 10^{9}$ in AF and $3.25 \times 10^{10} \pm 1.75 \times 10^{9}$ for CV-MSCs (Figure 7C). Viability assays were repeated testing AF- and CV-EXOs on SKOV-3 and OVCAR-3 cells in 2D and 3D culture systems. A significant reduction ($P < .05$) was induced in both cell lines by the exposure to AF-EXO, with values assessed around 27% ± 19.8 and 44.4% ± 1.6 for SKOV-3 and OVCAR-3, respectively (Figure 7E). Seventy-two hours of exposure to CV-EXO did not induce a significant decrease in cell viability, for none of the ovarian cancer cell lines tested. A slight reduction in SKOV-3 cell viability was noticed in the 3D system tested following exposure to AF-EXO (24% ± 5.6) and CV-EXO (20% ± 12), compared to untreated cells (CTRL) (Figure 7F). An opposite response was found in OVCAR-3 cells, where an increase in cell viability was evidenced after exposure to both, AF-EXO (20% ± 8.7) and CV-EXO (5% ± 14) compared to CTRL. We next evaluated the effect of AF- and CV-EXO to induce apoptosis in ovarian cancer cells. Most SKOV-3 cells were found in late

Downloaded from https://academic.oup.com/stcltm/article/13/7/693/7641993 by guest on 26 July 2024

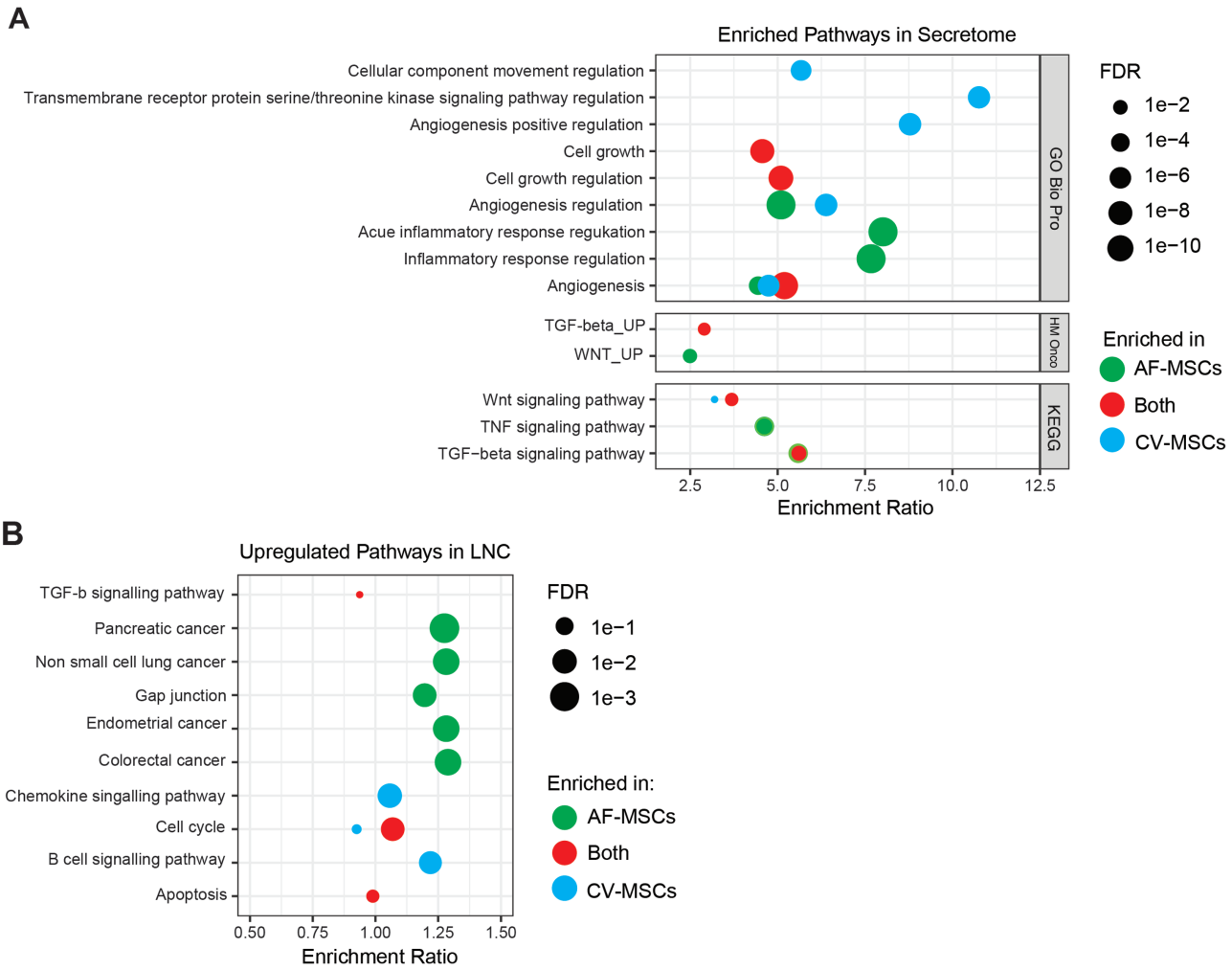

Figure 4. Pathway analysis of differentially regulated secreted proteins and lncRNA. (A) The enriched pathways in secretome show several functions of regulation in the cells, also it reports crucial signaling pathways (WNT, TNF, and TGF-β) involved in AF- and/or CV-MSCs. (B) The enrichment of upregulated pathways for lncRNA shows several cancer-related pathways in AF- and/or CV-MSCs.

apoptosis following the treatment with exosomes, with an increase of 54% ± 11.8 and 53% ± 15.6 after exposure to AF-EXO and CV-EXO respectively, compared to CTRL (untreated cells) (Figure 7G). Only a small percentage of SKOV-3 cells was revealed to be in early apoptosis upon exposure to AF-EXO, with an increase of 44% ± 30 in the luminescence signal (Figure 7H). Contrarily, OVCAR-3 cells showed an increase of 22% ± 21 and 20% ± 4.5 in the luminescence after treatment with CV- and AF-EXO, respectively.

Discussion

As a plastic cell population prone to altering or modulating the growth properties depending on the environment (ie, extracellular matrix, surrounding cells) they are exposed to, MSCs contribute to tissue homeostasis, repair by supporting angiogenesis, exerting an anti-apoptotic effect as well as modulating immune cell phenotypes.[24] The important MSC role in cancer biology, however, is currently disputed, due to their ability to both suppress and/or promote cancer properties.[25] MSCs isolated from adult (bone marrow and adipose tissue) and placental (umbilical cord and amniotic fluid) tissues have been the focus of recent studies supporting their anti-tumor potential, with particular emphasis on ovarian cancer.[24,26,27] In this work, we investigated the master regulators of the anti-tumor potential ascribed to MSCs in cells isolated from 2 therapeutically relevant gestational tissues, AF and CV. Our data demonstrate that the media conditioned by both cell lines contains not only pro-regenerative molecules (as widely established by the scientific community[28]) but also anti-tumor signatures.[29] Patient-derived MSCs underwent standard characterization in terms of morphology, proliferation, expression of established MSC markers, and differential potential,[30] which was followed by comparative transcriptomic analysis to evaluate their potential role in cancer regulation. Once confirmed AF- and CV-MSCs are good candidates against cancer initiation and progression, we tested their paracrine stimuli released as tools exert a cytotoxic effect on ovarian cancer cells. NGS analysis data showed a clear separation between the 2 cell lines analyzed, finding numerous genes highly expressed in both samples. DEGs analysis confirmed specific molecular traits for AF- and CV-MSCs, which align with the tissues and the time of gestation (between 15-20 and 10-13 weeks, respectively) they are harvested from[31] and depend on the role each of them play in supporting pregnancy.[32] However, no significant difference between the 2 cell lines was revealed by enrichment pathways analysis performed on those DEGs, aiming to define evidence to support their differential anticancer

Downloaded from https://academic.oup.com/stcltm/article/13/7/693/7641993 by guest on 26 July 2024

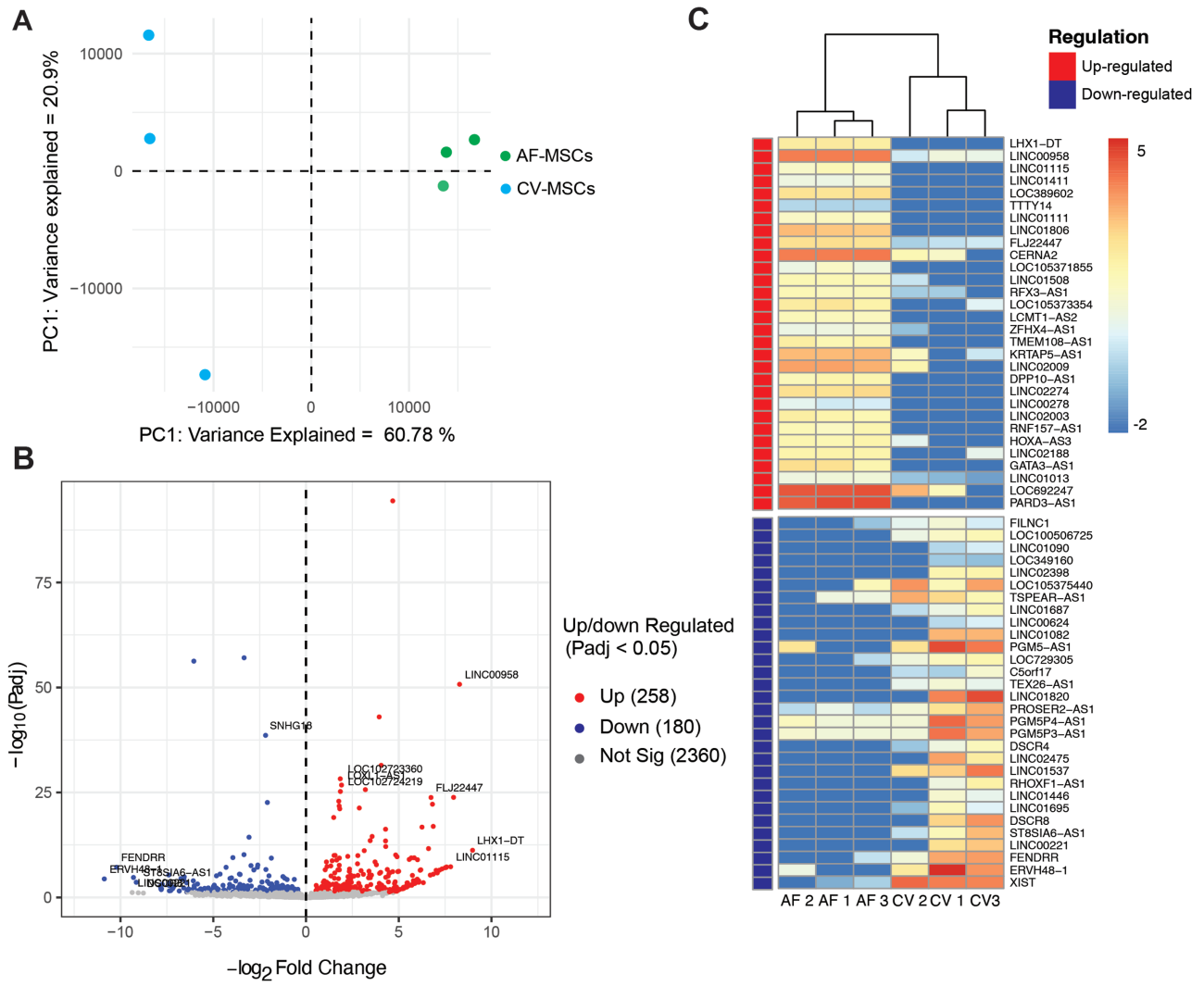

Figure 5. Secretome analysis differentially expressed lncRNA. (A) PCA plot shows the similarity between samples. (B) Volcano plot displaying the log fold change and *P*-value of lncRNA in AF samples against CV samples. Significantly upregulated and downregulated genes are reported (*P*adj < 0.05). Genes where *P*adj > 0.05 are also shown. (C) Hierarchical clustering heatmap showing top 30 up and top 30 downregulated lncRNA (*P* adjusted < .05) for AF- and CV-MSCs. Dendrograms show hierarchical clustering results.

potential. Our initial focus for the analysis was the genes encoding for secreted proteins, hypothesized to have a potential effect on surrounding cells and tissues. Following this approach, KEGG pathways analysis highlighted in AF- and CV-MSCs 3 pathways, typically associated with MSCs, which are known as controllers of the inflammatory processes. They include Wingless/Integrated (WNT), Tumor Growth Factor-beta (TFG-β), and Tumor Necrosis Factor (TNF) signaling pathways. The WNT family (with the specific involvement of the *Wnt5a*, *Wnt10a*, and *Wnt2a genes*) is known to control stem cell self-renewal and differentiation processes.[33] The TGF-β and TNF signaling pathways are well-known as immunosuppressive molecules able to activate epigenetic processes with the chromatin remodeling or the promotion of the DNA methylation.[34] These pathways confirm the literature reporting MSCs as strong inhibitors of pro-inflammatory immune cell populations.[35] On the other hand, these genes have been reported to play a role in numerous cancer types, including breast cancer,[36] hepatoma,[37] glioma,[38] and ovarian cancer,[39] where they exert a growth inhibitory effect through MSC-secreted prostaglandin E2 (PGE2), interleukin (IL)-6, indoleamine2,3-dioxygenase (IDO), TGF-β1, and nitric oxide.[38] The presence of these molecules has been confirmed by the enrichment GO BIO process we performed and according to literature produced by us and other groups, where they are considered as MSC-associated moieties involved in regulation of the inflammatory response.[40,41] In addition to this important function, the GO BIO process analysis also revealed pathways associated with angiogenesis regulation and endothelial cell proliferation, confirming MSCs role in gestational tissues to support embryo morphology and fetal development.[42] Molecules involved in angiogenesis are also known to regulate cancer and in some cases their activation is dual[16]: they exhibit tumor suppressive effects at early stages (by inhibiting cell cycle progression and promoting apoptosis) and represent carcinoma progressive elements (by increasing tumor invasiveness and the metastasis).[43,44] This is particularly true in the case of TGF-beta since it can act as a tumor suppressor or promoter.[45]

With the secretome analysis suggesting a potential anticancer effect for AF- and CV-MSCs, the role of paracrine signals released by them was experimentally validated on

Downloaded from https://academic.oup.com/stcltm/article/13/7/693/7641993 by guest on 26 July 2024

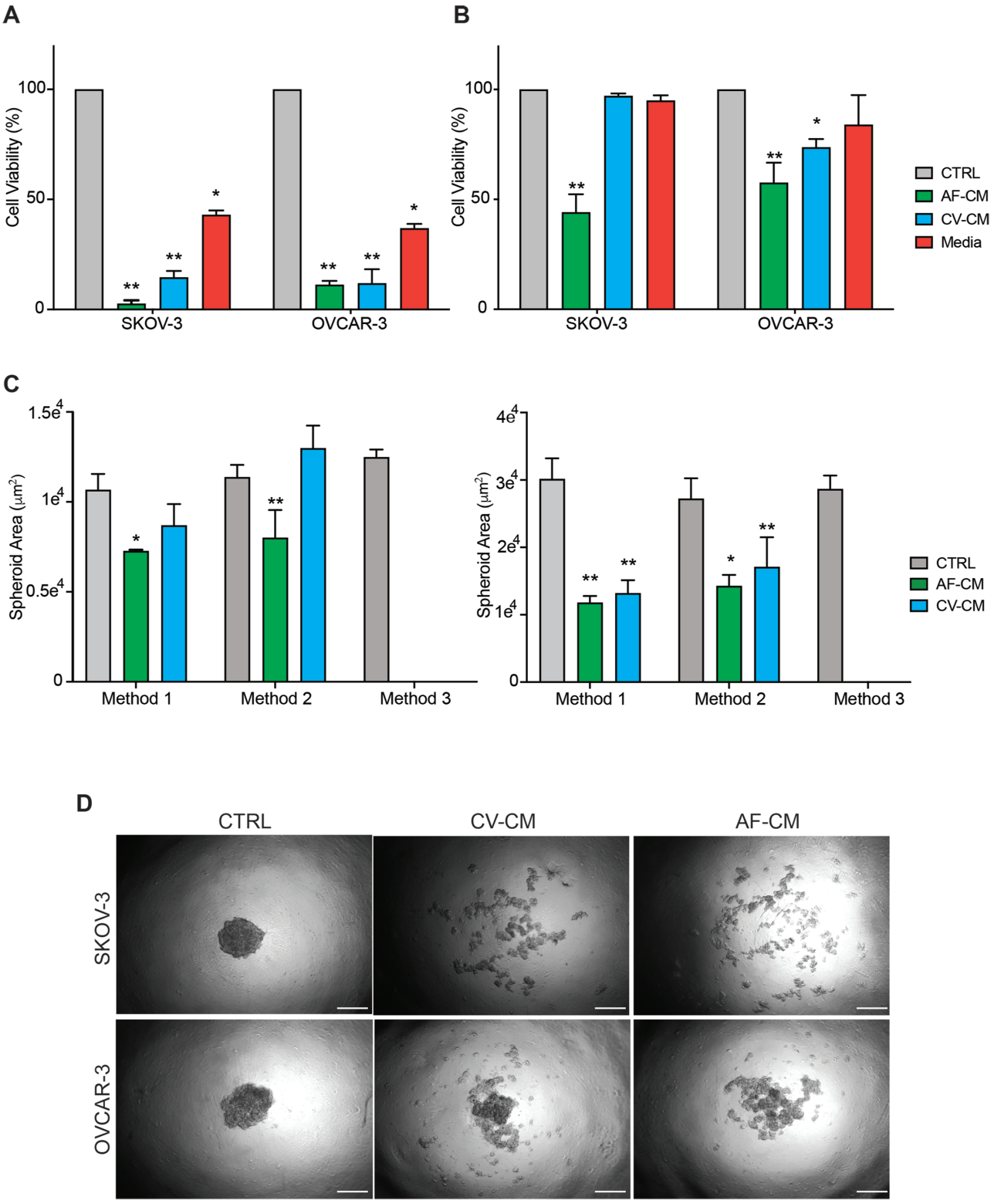

Figure 6. Effect of the media conditioned by AF- and CV-MSC on ovarian cancer cell viability and spheroid formation. Cell viability for SKOV-3 and OVCAR-3 after 72-hour exposure to CM obtained from AF- and CV-MSCs (depicted as AF-CM and CV-CM, respectively) in 2D (A) and 3D (B) culture. Untreated cancer cells (CTRL) and cells exposed to standard stem cell media (media) were included for comparison. Data are shown as average of 3 independent biological replicates ± SD. (C) Area (in μm^2) of spheroids produced by SKOV-3 and OVCAR-3 before (*Method* 1), after (*Method 2*), and during (*Method 3*) spheroid formation. Results are presented as average of 3 independent biological replicates ± SD. (*Significant and **highly significant differences with $P < .05$ and $P < .01$, respectively). (D) Representative brightfield images of fragmented spheroids produced by each cell line (SKOV-3 and OVCAR-3) upon exposure to AF- and CV-CM following *Method 3*.

Downloaded from https://academic.oup.com/stcltm/article/13/7/693/7641993 by guest on 26 July 2024

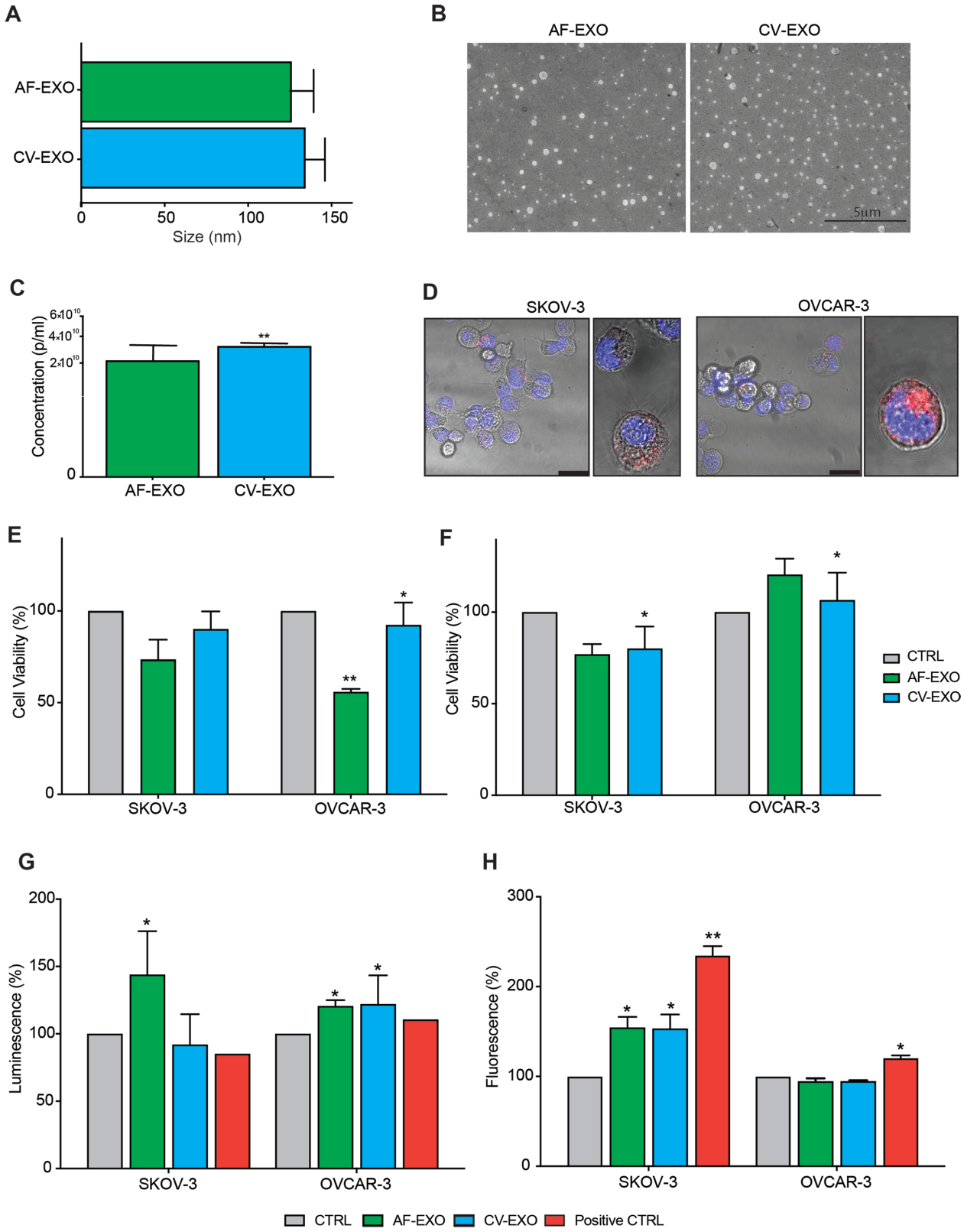

Figure 7. Effect of the exosomes produced by AF- and CV-MSCs on ovarian cancer cells. Size (in nm, A), morphology (B, from SEM imaging), and concentration (expressed as particles/mL, (C) of exosomes released by AF- and CV-MSCs (AF-EXO and CV-EXO, respectively). Size and concentration data obtained by NTA analysis. Data are presented as average of 3 biological replicates ± standard deviation. (D) Representative images showing the internalization into SKOV-3 and OVCAR-3 of fluorescently labeled AF-EXO. DAPI (nuclei), and DiD (exosomes, red). 10× and 20× Magnification, scale bar: 10 µm. SKOV-3 and OVCAR-3 cell viability (in percentage) after 72-hour exposure to AF-EXO and CV-EXO in 2D (D) and 3D (E) culture systems. The presence of cells in early apoptosis (F) was detected by a luminescent signal, whereas those in late apoptosis were identified by a fluorescent signal (G). Untreated cells and cells exposed to staurosporine were included as negative (CTRL) and positive controls, respectively. Data were expressed in percentage are represented as mean ± SD of 3 independent biological replicates compared to CTRL. Data is reported as average of 3 biological replicates ± SD (*$P < .05$, **$P < .01$).

Downloaded from https://academic.oup.com/stcltm/article/13/7/693/7641993 by guest on 26 July 2024

epithelial ovarian cancer cell lines (SKOV-3 and OVCAR-3) in 2D conditions. According to previously reported evidence on the cytotoxic effect of MSCs from other sources,[39,46,47] we observed a marked reduction in cell viability. This data could be correlated with an altered oxidative stress and a decreased mitochondrial membrane potential induced by MSCs in target cells,[28] or to the presence of immunosuppressive molecules (ie, interferon-gamma), which in turn promote cell apoptosis.[45] When SKOV-3 and OVCAR-3 cells were exposed to the CM by AF- and CV-MSCs in 3D culture system, strong cytotoxic action was found in AF-CM while only a slight (yet significant, $P < .5$) reduction in the viability of OVCAR-3 cells was also observed following the treatment with CV-CM. Discrepancies from 2D and 3D conditions can be explained by the spheroid-associated 3-dimensional rearrangement which partially recreates, in vitro, the in vivo tumor microenvironment.[48,49] Literature reports that during spheroid formation cancer cells acquire peculiar biological characteristics (such as hypoxia) that enable them to escape from applied therapeutic strategies.[50,51] To clarify this point, we decided to test the cytotoxic effect of AF- and CV-CM on ovarian cancer cells at different stages of spheroid formation, namely, before *(Method 1)*, after (*Method 2*) and during (*Method 3*) tridimensional arrangement. When cancer cells were treated with AF- and CV-CM during spheroid formation *(Method 3)*, we observed that 3D structure failed to form, suggesting that the presence of paracrine signals (ie, soluble factors and/or extracellular vesicles) within the CM may interfere with this process by impairing cellular cytoskeletal elements (ie, tubulins, vimentin, and dynamins).[52] During the formation of loose aggregates Tofani et al found low expression of 2 fundamental proteins in SKOV-3 and OVCAR-3, Fibronectin (FN) and β1-integrins which orchestrate initial cell aggregation and confer compact spheroid structure.[53] In line with our results, loose aggregates were formed as typical SKOV-3-based spheroids with mass-type morphology while OVCAR-3 cells formed grape-like spheroids.[54] The cohesion force between cells during spheroid formation is a determinant for chemoresistance in vivo by decreasing drug penetration. While OVCAR-3 cells are considered more aggressive than SKOV-3 because of the compactness of the spheroids they form, our results are in line with other studies showing a greater susceptibility compared to SKOV-3 in 3D treatments.[55] We speculate that the observed different behavior between the 2 ovarian cancer cell lines could depend on the properties like as changes in lipid metabolism or cytoskeletal remodeling targeting the cell surface that the cells adopt during hypoxia or shear stress.[52] Remarkably, we observed an increase in area and length of the spheroids formed by SKOV-3 cells, which is in agreement with existing literature showing when the oxygen concentration decreases, structural rearrangements occur in response to the microenvironment.[52]

To obtain a more comprehensive understanding of the action AF- and CV-MSCs exert against ovarian cancer, we analyzed lncRNAs as emerging tools able to regulate the initiation and the progression of several physiologic and pathological processes, including cancer.[56] We focused the attention on lncRNA as a class of non-coding RNAs able to regulate cellular functions, including gene transcription, enzymatic activity, and cell state maintenance and have a crucial role in developmental processes and disease.[49,57] LncRNAs identified in both cell lines (AF- and CV-MSCs) potentially target proteins involved in the cell cycle and apoptosis signaling pathways. The information provided by KEGG secretome enrichment analysis included TGF-β and TNF 2 cytokines considered proapoptotic agents. The 2 cytokines released by MSCs increase the expression of *P53* and *P21* genes which are involved in the apoptosis mechanisms through the interaction with the cyclin D1, blocking the cell cycle progression.[39] In AF-MSCs we found numerous cancer pathways, associated with the HOXA cluster genes (*Hoxa10-As, Hoxas2, Hoxas3, Hoxa11-As, Hotairm1*, and *Hottip*), a master regulator of the embryonic development and homeostasis maintenance mediated by MSCs but also implicated in the regulation of proliferation, apoptosis, migration, and invasion of cancer cells.[58] Based on the results obtained from lncRNA enrichment, we focused the attention on investigating whether this effect could be mediated by the extracellular vesicles they release. We subsequently investigated the role of exosomes since they are known to be important carriers of coding and non-coding RNA (ie, miRNA or lncRNA).[59] Due to the wide range of information they deliver to target cells (which depends on the properties of their parental cells), exosomes play a crucial role in all major biological processes, from homeostasis to apoptosis, from immunosuppression to immunomodulation, from metastasis to tumor inhibition cells.[60] Exosomes from AF- and CV-MSCs underwent standard characterization[61] and were administered to SKOV-3 and OVCAR-3 cells in both, 2D and 3D models. A marked reduction in viability was observed following AF-EXO exposure in 2D, supporting our hypothesis and further validating previously reported observations on the role AF-MSCs could play as promising source of therapeutics for cancer treatment.[39] To the slight reduction in viability was noticed following CV-EXO administration corresponds to an increase in the percentage of apoptotic cells, confirming the potential role of the lncRNAs identified by NGS analysis. A different trend was also found in 3D, whereby an increase in viability was observed for OVCAR-3 cells upon exposure to AF- and CV-EXOs. Once again, this observation can be explained considering the changes in the microenvironment induced by the interaction of numerous key elements of a multistep process of tumor development,[62] and the capability of OVCAR-3 cells to easily adapt to it by enhancing the resistance to anti-cancer drugs compared to monolayers (2D model).[63] Furthermore, spheroids produced by OVCAR-3 have been reported to display cancer stem cell characteristics, such as self-renewal, the ability to produce differentiated progeny, and gene expression. According to viability 3D model results, we observed a prevalence of late apoptosis in SKOV-3 cells and a slight OVCAR-3 population in early apoptosis upon CV- and AF-EXO treatment.

Limitations of the study

Taken together, data obtained from this study supports our hypothesis that MSCs from gestational tissues, particularly those derived from the amniotic fluid and chorionic villi, retain anti-cancer effects that are mediated by regulatory moieties they release. Despite the substantial work conducted, both experimentally and in silico, we feel obliged to point out some limitations. First, while the datasets generated here are promising they call for a subsequent investigation based on a larger number of patient-derived samples to provide stronger evidence and draw a definitive conclusion. While we acknowledge interpatient variability, the set-up of the experimental design was based on the Good Laboratory Standards

Downloaded from https://academic.oup.com/stcltm/article/13/7/693/7641993 by guest on 26 July 2024

for Clinical Next-Generation Sequencing testing[64,65] which recommends at least 3 samples to establish precision adequately, as well as on sample availability at the time the study was conducted. This number is also deemed sufficient in previously reported studies performing transcriptomic profiling of stem cells from several sources (neural, amniotic fluid, hair follicles, etc.). Second, transcriptomic data were validated in vitro through 2D and 3D conditions. While 3D culture systems are gaining momentum in the development of cancer therapeutics[66] preclinical studies would provide evidence of the anti-cancer potential of AF- and CV-MSCs (and their secretome) in a system that more closely recapitulates the complexity of the tumor microenvironment. We anticipate, however, that building on this work, future studies evaluating the anti-cancer potential of the secretome of AF- and CV-MSCs will be performed in mouse models of syngeneic ovarian cancer optimized in the lab[67] to provide additional insights on the biological effect in complex systems. Finally, moving forward, we are committed to providing a comprehensive characterization (in terms of proteomic, lipidomic, and transcriptomic profile) of the exosomes released by AF- and CV-MSCs, to identify specific targeting moieties as well as master regulators of the cytotoxic and inhibitory effect observed.

With the opportunity to identify exosome inherent targeting specificity and mechanisms of action, this approach offers the advantage of developing ad hoc tailored biomimetic therapeutics for cancer and other degenerative disorders, with the potential to overcome the current limitations in exosome manufacturing, including the yield and molecular complexity. The translation of these findings into clinical applications demands careful consideration of regulatory aspects, long-term safety assessments, and optimization of delivery methods.

Conclusion

Transcriptomic data presented in this work confirm the hypothesized role of the paracrine signals (including extracellular vesicles) as powerful tools used by AF- and CV-MSCs to achieve the important mission of communication with surrounding cells, and to maintaining tissue homeostasis, which is particularly crucial during embryo development. Our finding suggests AF-MSCs (and secretome) display a more marked anti-cancer effect than their chorionic villi-derived counterparts. This difference likely depends on the role AF and CV play in supporting embryo development and is the natural consequence of signature genes found upregulated in AF-MSCs that play a dual role, as they are critical in regulating embryonic growth as well as several cancer pathways (ie, the HOXA gene cluster). Indeed, similarities between early embryo development and tumorigenesis exist, with respect to cell invasive behavior and genetic/epigenetic regulation[68,69] which provide the opportunity to exploit developmental biology to identify potential targets against tumor initiation and progression.[1] This work not only highlights the anti-tumor potential of MSCs from gestational tissues. It also sheds light on the different responses SKOV-3 and OVCAR-3 activate as coping molecular mechanisms against the MSCs derivatives. Based on this framework, further studies will be required to dissect the molecular moieties contained in exosomes (not limited to the RNA cargo) that are directly involved in the anti-apoptotic and inhibitory effect observed in this context.

Acknowledgements

B.C. received support from the Sêr Cymru II programme, funded by the European Commission through the Horizon 2020 Marie Skłodowska-Curie Actions (MSCA) COFUND scheme and the Welsh European Funding Office (WEFO) under the European Regional Development Fund (ERDF) and Houston Methodist Research Institute (United States).

Author Contributions

Salvatore Vaiasicca conducted experiments and wrote the manuscript, Gianmarco Melone contributed to data interpretation and manuscript drafting, David W. James and Marcos Quintela conducted bioinformatic analyses and contributed to manuscript drafting; Seydou Yao supervised exosome isolation, Jing Xiao performed SEM analysis and differentiation studies, Richard H. Finnell and Robert S. Conlan imputed to project management and reviewed the draft manuscript, Lewis W. Francis supervised laboratory work, bioinformatic analysis and was involved in manuscript drafting, and Bruna Corradetti conceived and designed the project, supervised research activities, and wrote the manuscript.

Conflicts of Interest

The authors declare no potential conflicts of interest.

Ethics Approval and Consent to Participate

This study was conducted on cells isolated at the Cytogenetic Laboratory Children's Hospital Salesi (Ancona, Italy) in accordance with the Declaration of Helsinki. Samples were obtained for prenatal diagnosis upon informed consent signature from patients for the use of tissue for research purposes (based on d.l.gs. 196/2003-101/2018 and privacy protection 8/2016) and ethical approval by the Regional Institutional Review Board (Comitato Etico Regione Marche, Ref. UE 679/2016) on 07/29/2019).

Data Availability

Raw and processed datasets have been deposited in NCBI's Gene Expression Omnibus (GEO) (https://www.ncbi.nlm.nih.gov/geo/query/acc.cgi?&acc=GSE240855).

Supplementary Material

Supplementary material is available at *Stem Cells Translational Medicine* online.

References

1. Corradetti B, Dogra P, Pisano S, et al. Amphibian regeneration and mammalian cancer: Similarities and contrasts from an evolutionary biology perspective: comparing the regenerative potential of mammalian embryos and urodeles to develop effective strategies

Downloaded from https://academic.oup.com/stcltm/article/13/7/693/7641993 by guest on 26 July 2024

against human cancer. *Bioessays*. 2021;43(7):e2000339. https://doi.org/10.1002/bies.202000339
2. Ghimire S, Mantziou V, Moris N, Martinez Arias A. Human gastrulation: the embryo and its models. *Dev Biol*. 2021;474:100-108. https://doi.org/10.1016/j.ydbio.2021.01.006
3. Wang H, Yang GX, Hu Y, et al. Comprehensive human amniotic fluid metagenomics supports the sterile womb hypothesis. *Sci Rep*. 2022;12(1):6875. https://doi.org/10.1038/s41598-022-10869-7
4. Abe Y, Ochiai D, Masuda H, et al. In utero amniotic fluid stem cell therapy protects against myelomeningocele via spinal cord coverage and hepatocyte growth factor secretion. *Stem Cells Transl Med*. 2019;8(11):1170-1179. https://doi.org/10.1002/sctm.19-0002
5. Abe Y, Ochiai D, Sato Y, et al. Amniotic fluid stem cells as a novel strategy for the treatment of fetal and neonatal neurological diseases. *Placenta*. 2021;104:247-252. https://doi.org/10.1016/j.placenta.2021.01.009
6. Poloni A, Maurizi G, Babini L, et al. Human mesenchymal stem cells from chorionic villi and amniotic fluid are not susceptible to transformation after extensive in vitro expansion. *Cell Transplant*. 2011;20(5):643-654. https://doi.org/10.3727/096368910X536518
7. Sessarego N, Parodi A, Podesta M, et al. Multipotent mesenchymal stromal cells from amniotic fluid: solid perspectives for clinical application. *Haematologica*. 2008;93(3):339-346. https://doi.org/10.3324/haematol.11869
8. He N, Kong Y, Lei X, et al. MSCs inhibit tumor progression and enhance radiosensitivity of breast cancer cells by down-regulating Stat3 signaling pathway. *Cell Death Dis*. 2018;9(10):1026. https://doi.org/10.1038/s41419-018-0949-3
9. Balbous A, Cortes U, Guilloteau K, et al. A mesenchymal glioma stem cell profile is related to clinical outcome. *Oncogenesis*. 2014;3(3):e91. https://doi.org/10.1038/oncsis.2014.5
10. Chowdhury R, Webber JP, Gurney M, et al. Cancer exosomes trigger mesenchymal stem cell differentiation into pro-angiogenic and pro-invasive myofibroblasts. *Oncotarget*. 2015;6(2):715-731. https://doi.org/10.18632/oncotarget.2711
11. Maacha S, Bhat AA, Jimenez L, et al. Extracellular vesicles-mediated intercellular communication: roles in the tumor microenvironment and anti-cancer drug resistance. *Mol Cancer*. 2019;18(1):55. https://doi.org/10.1186/s12943-019-0965-7
12. Pitt JM, Kroemer G, Zitvogel L. Extracellular vesicles: masters of intercellular communication and potential clinical interventions. *J Clin Invest*. 2016;126(4):1139-1143. https://doi.org/10.1172/JCI87316
13. Sharma A. Role of stem cell derived exosomes in tumor biology. *Int J Cancer*. 2018;142(6):1086-1092. https://doi.org/10.1002/ijc.31089
14. Tetta C, Ghigo E, Silengo L, Deregibus MC, Camussi G. Extracellular vesicles as an emerging mechanism of cell-to-cell communication. *Endocrine*. 2013;44(1):11-19. https://doi.org/10.1007/s12020-012-9839-0
15. Kim D, Paggi JM, Park C, Bennett C, Salzberg SL. Graph-based genome alignment and genotyping with HISAT2 and HISAT-genotype. *Nat Biotechnol*. 2019;37(8):907-915. https://doi.org/10.1038/s41587-019-0201-4
16. Varas-Godoy M, Rice G, Illanes SE. The crosstalk between ovarian cancer stem cell niche and the tumor microenvironment. *Stem Cells Int*. 2017;2017:5263974. https://doi.org/10.1155/2017/5263974
17. Vaiasicca S, Melone G, James DW, et al. Transcriptomic analysis of stem cells from chorionic villi uncovers the impact of chromosomes 2, 6 and 22 in the clinical manifestations of Down syndrome. *Stem Cell Res Ther*. 2023;14(1):265. https://doi.org/10.1186/s13287-023-03503-4
18. Love MI, Huber W, Anders S. Moderated estimation of fold change and dispersion for RNA-seq data with DESeq2. *Genome Biol*. 2014;15(12):550. https://doi.org/10.1186/s13059-014-0550-8
19. Uhlen M, Karlsson MJ, Hober A, et al. The human secretome. *Sci Signal*. 2019;12(609):eaaz0274. https://doi.org/10.1126/scisignal.aaz0274
20. Kanehisa M, Sato Y, Kawashima M, Furumichi M, Tanabe M. KEGG as a reference resource for gene and protein annotation. *Nucleic Acids Res*. 2016;44(D1):D457-D462. https://doi.org/10.1093/nar/gkv1070
21. Carbon S, Douglass E, et al. The Gene Ontology resource: enriching a GOld mine. *Nucleic Acids Res*. 2021;49(D1):D325-DD34.
22. Liberzon A, Birger C, Thorvaldsdottir H, et al. The Molecular Signatures Database (MSigDB) hallmark gene set collection. *Cell Syst*. 2015;1(6):417-425. https://doi.org/10.1016/j.cels.2015.12.004
23. Han J, Liu S, Sun Z, et al. LncRNAs2Pathways: identifying the pathways influenced by a set of lncRNAs of interest based on a global network propagation method. *Sci Rep*. 2017;7:46566. https://doi.org/10.1038/srep46566
24. Melzer C, von der Ohe J, Hass R. MSC stimulate ovarian tumor growth during intercellular communication but reduce tumorigenicity after fusion with ovarian cancer cells. *Cell Commun Signal*. 2018;16(1):67. https://doi.org/10.1186/s12964-018-0279-1
25. Hong IS, Lee HY, Kang KS. Mesenchymal stem cells and cancer: friends or enemies? *Mutat Res*. 2014;768:98-106. https://doi.org/10.1016/j.mrfmmm.2014.01.006
26. Khalil C, Moussa M, Azar A, et al. Anti-proliferative effects of mesenchymal stem cells (MSCs) derived from multiple sources on ovarian cancer cell lines: an in-vitro experimental study. *J Ovarian Res*. 2019;12(1):70. https://doi.org/10.1186/s13048-019-0546-9
27. Zheng L, Zhang D, Chen X, et al. Antitumor activities of human placenta-derived mesenchymal stem cells expressing endostatin on ovarian cancer. *PLoS One*. 2012;7(7):e39119. https://doi.org/10.1371/journal.pone.0039119
28. Han Y, Li X, Zhang Y, Chang F, Ding J. Mesenchymal stem cells for regenerative medicine. *Cells*. 2019;8(8):1-32.
29. Bracher M, Pilkington GJ, Hanemann CO, Pilkington K. A systematic approach to review of in vitro methods in brain tumour research (SAToRI-BTR): development of a preliminary checklist for evaluating quality and human relevance. *Front Bioeng Biotechnol*. 2020;8:936. https://doi.org/10.3389/fbioe.2020.00936
30. Dominici M, Le Blanc K, Mueller I, et al. Minimal criteria for defining multipotent mesenchymal stromal cells. The International Society for Cellular Therapy position statement. *Cytotherapy*. 2006;8(4):315-317. https://doi.org/10.1080/14653240600855905
31. Rosner M, Kolbe T, Voronin V, Hengstschlager M. Amniotic fluid stem cells and the cell source repertoire for non-invasive prenatal testing. *Stem Cell Rev Rep*. 2022;18(4):1366-1371. https://doi.org/10.1007/s12015-021-10228-5
32. Fitzsimmons ED, Bajaj T. *Embryology, Amniotic Fluid*. StatPearls Publishing. 2024.
33. Takam Kamga P, Bazzoni R, Dal Collo G, et al. The role of notch and wnt signaling in MSC communication in normal and leukemic bone marrow niche. *Front Cell Dev Biol*. 2020;8:599276. https://doi.org/10.3389/fcell.2020.599276
34. Liu F, Qiu H, Xue M, et al. MSC-secreted TGF-beta regulates lipopolysaccharide-stimulated macrophage M2-like polarization via the Akt/FoxO1 pathway. *Stem Cell Res Ther*. 2019;10(1):345. https://doi.org/10.1186/s13287-019-1447-y
35. Yang G, Fan X, Liu Y, et al. Immunomodulatory mechanisms and therapeutic potential of mesenchymal stem cells. *Stem Cell Rev Rep*. 2023;19(5):1214-1231.
36. Sun B, Roh KH, Park JR, et al. Therapeutic potential of mesenchymal stromal cells in a mouse breast cancer metastasis model. *Cytotherapy*. 2009;11(3):289-98, 1 p following 298. https://doi.org/10.1080/14653240902807026
37. Qiao L, Xu Z, Zhao T, et al. Suppression of tumorigenesis by human mesenchymal stem cells in a hepatoma model. *Cell Res*. 2008;18(4):500-507. https://doi.org/10.1038/cr.2008.40
38. Jiao H, Guan F, Yang B, et al. Human amniotic membrane derived-mesenchymal stem cells induce C6 glioma apoptosis in vivo through the Bcl-2/caspase pathways. *Mol Biol Rep*. 2012;39(1):467-473. https://doi.org/10.1007/s11033-011-0760-z

Downloaded from https://academic.oup.com/stcltm/article/13/7/693/7641993 by guest on 26 July 2024

39. Gholizadeh-Ghaleh Aziz S, Fardyazar Z, Pashaiasl M. The human amniotic fluid mesenchymal stem cells therapy on, SKOV3, ovarian cancer cell line. *Mol Genet Genomic Med*. 2019;7(7):e00726. https://doi.org/10.1002/mgg3.726
40. Javan MR, Khosrojerdi A, Moazzeni SM. New insights into implementation of mesenchymal stem cells in cancer therapy: prospects for anti-angiogenesis treatment. *Front Oncol*. 2019;9:840. https://doi.org/10.3389/fonc.2019.00840
41. Corradetti B, Taraballi F, Minardi S, et al. Chondroitin sulfate immobilized on a biomimetic scaffold modulates inflammation while driving chondrogenesis. *Stem Cells Transl Med*. 2016;5(5):670-682. https://doi.org/10.5966/sctm.2015-0233
42. Hsieh JY, Wang HW, Chang SJ, et al. Mesenchymal stem cells from human umbilical cord express preferentially secreted factors related to neuroprotection, neurogenesis, and angiogenesis. *PLoS One*. 2013;8(8):e72604. https://doi.org/10.1371/journal.pone.0072604
43. Syed V. TGF-beta signaling in cancer. *J Cell Biochem*. 2016;117(6):1279-1287. https://doi.org/10.1002/jcb.25496
44. Wu X, Zhao J, Ruan Y, et al. Sialyltransferase ST3GAL1 promotes cell migration, invasion, and TGF-beta1-induced EMT and confers paclitaxel resistance in ovarian cancer. *Cell Death Dis*. 2018;9(11):1102. https://doi.org/10.1038/s41419-018-1101-0
45. Kumari A, Shonibare Z, Monavarian M, et al. TGFbeta signaling networks in ovarian cancer progression and plasticity. *Clin Exp Metastasis*. 2021;38(2):139-161. https://doi.org/10.1007/s10585-021-10077-z
46. Hui L, Chen Y. Tumor microenvironment: sanctuary of the devil. *Cancer Lett*. 2015;368(1):7-13. https://doi.org/10.1016/j.canlet.2015.07.039
47. Gao T, Yu Y, Cong Q, et al. Human mesenchymal stem cells in the tumour microenvironment promote ovarian cancer progression: the role of platelet-activating factor. *BMC Cancer*. 2018;18(1):999. https://doi.org/10.1186/s12885-018-4918-0
48. Bracher M, Pilkington GJ, Pilkington K. Systematic reviews and quality appraisal of in vitro cancer studies: investigation of current practice. *Anticancer Res*. 2021;41(11):5377-5391. https://doi.org/10.21873/anticanres.15350
49. Reza A, Choi YJ, Yasuda H, Kim JH. Human adipose mesenchymal stem cell-derived exosomal-miRNAs are critical factors for inducing anti-proliferation signalling to A2780 and SKOV-3 ovarian cancer cells. *Sci Rep*. 2016;6:38498.
50. Lee JM, Mhawech-Fauceglia P, Lee N, et al. A 3-dimensional microenvironment alters protein expression and chemosensitivity of epithelial ovarian cancer cells in vitro. *Lab Invest*. 2013;93(5):528-542. https://doi.org/10.1038/labinvest.2013.41
51. Liu M, Zhang X, Long C, et al. Collagen-based 3-dimensional culture microenvironment promotes epithelial to mesenchymal transition and drug resistance of human ovarian cancer in vitro. *RSC Adv*. 2018;8(16):8910-8919. https://doi.org/10.1039/c7ra13742g
52. Bileck A, Bortel P, Kriz M, et al. Inward outward signaling in ovarian cancer: morpho-phospho-proteomic profiling upon application of hypoxia and shear stress characterizes the adaptive plasticity of OVCAR-3 and SKOV-3 cells. *Front Oncol*. 2021;11:746411. https://doi.org/10.3389/fonc.2021.746411
53. Tofani LB, Abriata JP, Luiz MT, Marchetti JM, Swiech K. Establishment and characterization of an in vitro 3D ovarian cancer model for drug screening assays. *Biotechnol Prog*. 2020;36(6):e3034. https://doi.org/10.1002/btpr.3034
54. Kenny PA, Lee GY, Myers CA, et al. The morphologies of breast cancer cell lines in 3-dimensional assays correlate with their profiles of gene expression. *Mol Oncol*. 2007;1(1):84-96. https://doi.org/10.1016/j.molonc.2007.02.004
55. Giannakouros P, Comamala M, Matte I, Rancourt C, Piche A. MUC16 mucin (CA125) regulates the formation of multicellular aggregates by altering beta-catenin signaling. *Am J Cancer Res*. 2015;5(1):219-230.
56. Loganathan T, Doss CG. Non-coding RNAs in human health and disease: potential function as biomarkers and therapeutic targets. *Funct Integr Genomics*. 2023;23(1):33.
57. Quinn JJ, Chang HY. Unique features of long non-coding RNA biogenesis and function. *Nat Rev Genet*. 2016;17(1):47-62. https://doi.org/10.1038/nrg.2015.10
58. Wang J, Su Z, Lu S, et al. LncRNA HOXA-AS2 and its molecular mechanisms in human cancer. *Clin Chim Acta*. 2018;485:229-233. https://doi.org/10.1016/j.cca.2018.07.004
59. Sun Z, Yang S, Zhou Q, et al. Emerging role of exosome-derived long non-coding RNAs in tumor microenvironment. *Mol Cancer*. 2018;17(1):82. https://doi.org/10.1186/s12943-018-0831-z
60. Chopra N, Dutt Arya B, Jain N, et al. Biophysical characterization and drug delivery potential of exosomes from human Wharton's Jelly-derived mesenchymal stem cells. *ACS Omega*. 2019;4(8):13143-13152. https://doi.org/10.1021/acsomega.9b01180
61. Tan SHS, Wong JRY, Sim SJY, et al. Mesenchymal stem cell exosomes in bone regenerative strategies—a systematic review of preclinical studies. *Mater Today Biol*. 2020;7:100067. https://doi.org/10.1016/j.mtbio.2020.100067
62. Thoma CR, Zimmermann M, Agarkova I, Kelm JM, Krek W. 3D cell culture systems modeling tumor growth determinants in cancer target discovery. *Adv Drug Deliv Rev*. 2014;69-70:29-41. https://doi.org/10.1016/j.addr.2014.03.001
63. Gunay G, Kirit HA, Kamatar A, et al. The effects of size and shape of the ovarian cancer spheroids on the drug resistance and migration. *Gynecol Oncol*. 2020;159(2):563-572. https://doi.org/10.1016/j.ygyno.2020.09.002
64. Aziz N, Zhao Q, Bry L, et al. College of American Pathologists' laboratory standards for next-generation sequencing clinical tests. *Arch Pathol Lab Med*. 2015;139(4):481-493. https://doi.org/10.5858/arpa.2014-0250-CP
65. Kim J, Park WY, Kim NKD, et al; Molecular Pathology Study Group of Korean Society of Pathologists. Good laboratory standards for clinical next-generation sequencing cancer panel tests. *J Pathol Transl Med*. 2017;51(3):191-204. https://doi.org/10.4132/jptm.2017.03.14
66. Manduca N, Maccafeo E, De Maria R, Sistigu A, Musella M. 3D cancer models: one step closer to in vitro human studies. *Front Immunol*. 2023;14:1175503. https://doi.org/10.3389/fimmu.2023.1175503
67. Pisano S, Lenna S, Healey GD, et al. Assessment of the immune landscapes of advanced ovarian cancer in an optimized in vivo model. *Clin Transl Med*. 2021;11(10):e551. https://doi.org/10.1002/ctm2.551
68. Ma Y, Zhang P, Wang F, et al. The relationship between early embryo development and tumourigenesis. *J Cell Mol Med*. 2010;14(12):2697-2701. https://doi.org/10.1111/j.1582-4934.2010.01191.x
69. Cofre J, Saalfeld K. The first embryo, the origin of cancer and animal phylogeny. I. A presentation of the neoplastic process and its connection with cell fusion and germline formation. *Front Cell Dev Biol*. 2022;10:1067248. https://doi.org/10.3389/fcell.2022.1067248

Downloaded from https://academic.oup.com/stcltm/article/13/7/693/7641993 by guest on 26 July 2024